

Review

Fluorescent Organic Small Molecule Probes for Bioimaging and Detection Applications

Yufei Yang, Fucheng Gao, Yandong Wang, Hui Li, Jie Zhang *, Zhiwei Sun * and Yanyan Jiang *

Key Laboratory for Liquid–Solid Structural Evolution and Processing of Materials, Ministry of Education, Shandong University, Jinan 250061, China

* Correspondence: jnzhangjie@sdu.edu.cn (J.Z.); sun_zhiwei@mail.sdu.edu.cn (Z.S.);

yanyan.jiang@sdu.edu.cn (Y.J.); Tel.: +86-15864027426 (J.Z.); +86-13622005679 (Z.S.); +86-17865551290 (Y.J.)

Abstract: The activity levels of key substances (metal ions, reactive oxygen species, reactive nitrogen, biological small molecules, etc.) in organisms are closely related to intracellular redox reactions, disease occurrence and treatment, as well as drug absorption and distribution. Fluorescence imaging technology provides a visual tool for medicine, showing great potential in the fields of molecular biology, cellular immunology and oncology. In recent years, organic fluorescent probes have attracted much attention in the bioanalytical field. Among various organic fluorescent probes, fluorescent organic small molecule probes (FOSMPs) have become a research hotspot due to their excellent physicochemical properties, such as good photostability, high spatial and temporal resolution, as well as excellent biocompatibility. FOSMPs have proved to be suitable for in vivo bioimaging and detection. On the basis of the introduction of several primary fluorescence mechanisms, the latest progress of FOSMPs in the applications of bioimaging and detection is comprehensively reviewed. Following this, the preparation and application of fluorescent organic nanoparticles (FONPs) that are designed with FOSMPs as fluorophores are overviewed. Additionally, the prospects of FOSMPs in bioimaging and detection are discussed.



Citation: Yang, Y.; Gao, F.; Wang, Y.; Li, H.; Zhang, J.; Sun, Z.; Jiang, Y. Fluorescent Organic Small Molecule Probes for Bioimaging and Detection Applications. *Molecules* **2022**, *27*, 8421. <https://doi.org/10.3390/molecules27238421>

Academic Editor: Yongzhong Bian

Received: 16 October 2022

Accepted: 21 November 2022

Published: 1 December 2022

Publisher's Note: MDPI stays neutral with regard to jurisdictional claims in published maps and institutional affiliations.



Copyright: © 2022 by the authors. Licensee MDPI, Basel, Switzerland. This article is an open access article distributed under the terms and conditions of the Creative Commons Attribution (CC BY) license (<https://creativecommons.org/licenses/by/4.0/>).

Keywords: fluorescent organic small molecules; bioimaging; detection; recognition mechanisms; fluorescent organic nanoparticles

1. Introduction

The key substances inside the human body, including metal ions [1], biological small molecules [2,3], reactive oxygen species [4–6] and reactive nitrogen [7,8], are closely related to biological events, regulating physiological functions and metabolism. For instance, metal ions (e.g., Fe^{3+} , Na^+ , Al^{3+} and Mg^{2+}) play important regulatory roles in metabolism and osmolality [9–11]. Biological small molecules, such as homocysteine (Hcy), cysteine (Cys) and glutathione (GSH) participate in metabolism and redox reactions [12–14]. The content of reactive oxygen species and reactive nitrogen reflects many pathological states, especially the development of cancer [15–18]. Therefore, monitoring the levels of these substances is helpful for understanding human health status.

With the development of in vivo imaging technology, more and more tracer techniques have been applied in biomedical research. Traditional tracing methods are usually required to remove tissues from the body, which cannot realize the real-time dynamic monitoring of the target substances. Currently, the commonly used in vivo tracer techniques include radionuclide imaging, magnetic resonance imaging (MRI), optical imaging and so on [19]. Radionuclide imaging can achieve quantitative and localization analysis of cells, but it has the shortcomings of low spatial resolution and the need of expensive equipment [20,21]. MRI with high spatial and temporal resolution enables monitoring of changes in cellular function, but this technique faces the problem of long imaging time [22]. In vivo luminescence imaging is a non-invasive technology, including bioluminescence imaging (BLI)

and fluorescence imaging, mainly used to study gene expression and cell activity. Compared with BLI, the signal of fluorescence imaging is stronger and the detection accuracy is higher [23–25]. At present, *in vivo* fluorescence imaging has become a hotspot in biomedical research due to its advantages of low toxicity, high spatiotemporal resolution and utilization of an inexpensive instrument [26–28]. For example, fluorescent dye indocyanine green (ICG) imaging has been used in a variety of abdominal surgery applications, such as lymph node localization, ureteral detection and tumor identification [29]. In recent years, some fluorescent probes with high specificity have also been developed and used for *in vivo* imaging [30–32].

To date, many types of fluorescent probes, such as fluorescent organics [33–36], fluorescent proteins [37], inorganic nanoparticles [38,39] and semiconductor polymer nanoparticles [40,41] have been developed and widely used in bioimaging. Fluorescent proteins can be generated by cells themselves through genetic engineering, which is convenient for *in vivo* imaging. However, they are hard to metabolize in the body. Inorganic nanoparticles have good spectral properties and light stability, but the biological toxicity limits their application in bioimaging. Semiconductor polymer nanoparticles have high fluorescence brightness, but slow metabolism causes them to accumulate in the liver. Comparatively, fluorescent organic small molecule probes (FOSMPs) attracted more attention because of their controllable synthesis, stable luminescence, good biocompatibility, sensitive response and high signal-to-noise ratio [42,43]. When applied to imaging, the photochemical properties of FOSMPs are generally more stable than other types of probes. Additionally, small molecules also help to achieve higher fluorophore density and spatial resolution. Therefore, a large number of FOSMPs have been designed and applied to detect substances in various matrix [44–51]. Fluorescent organic nanoparticles (FONPs), which were designed with FOSMPs as fluorophores, show the ability to build a multifunctional biosensing platform through surface functionalization and drug encapsulation [52]. A summary of the progress on the applications of FOSMPs in bioimaging and detection is of significance for the development of new diagnostic tools. As far as we know, there are no special reviews focusing on this field. This review focuses on the application of FOSMPs and FONPs in bioimaging and detection, including the fluorescence mechanism, detection principle, representative examples and development prospect. This review aims to provide a reference for the development of new tools and strategies for *in vivo* biosensing of key substances by using FOSMPs.

2. FOSMPs for Bioimaging and Detection

Fluorescence is the phenomenon that electrons return from the first singlet state to the ground state with concomitant energy release in the form of light. The characteristics of the fluorescent probes such as excitation and emission wavelength, intensity, lifetime and polarization are easily influenced by the environment conditions, thereby providing sensitive signals for the tracking and monitoring of analytes [53–58]. The structure of FOSMPs is mainly composed of three parts: the recognition group, the fluorophore, and the linking group (linker) (Figure 1). The recognition group endows the fluorescent probe with detection selectivity. The fluorophore provides the signal response when the probe recognizes the target. The linker connects the recognition group and the fluorophore and is not necessary for the fluorescent probe.

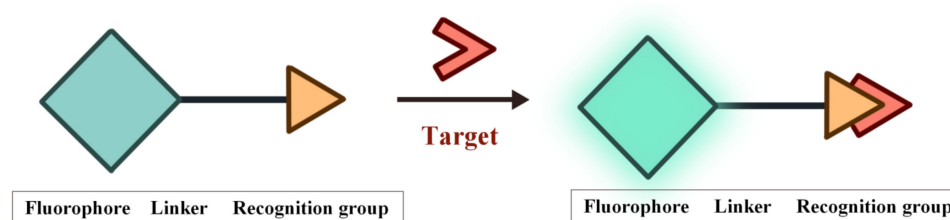


Figure 1. The structure of FOSMPs and its recognition of the target.

As shown in Figure 2, according to the interaction manner between FOSMPs and targets, the recognition mechanisms can be divided into five types: photo-induced electron transfer (PET), intramolecular charge transfer (ICT), fluorescence resonance energy transfer (FRET), excited state intramolecular proton transfer (ESIPT) and aggregation-induced emission (AIE). Based on these recognition mechanisms, various FOSMPs for bioimaging and detection have been developed, as listed in Table 1. In the following, the applications of FOSMPs in bioimaging and analysis based on these recognition mechanisms are reviewed.

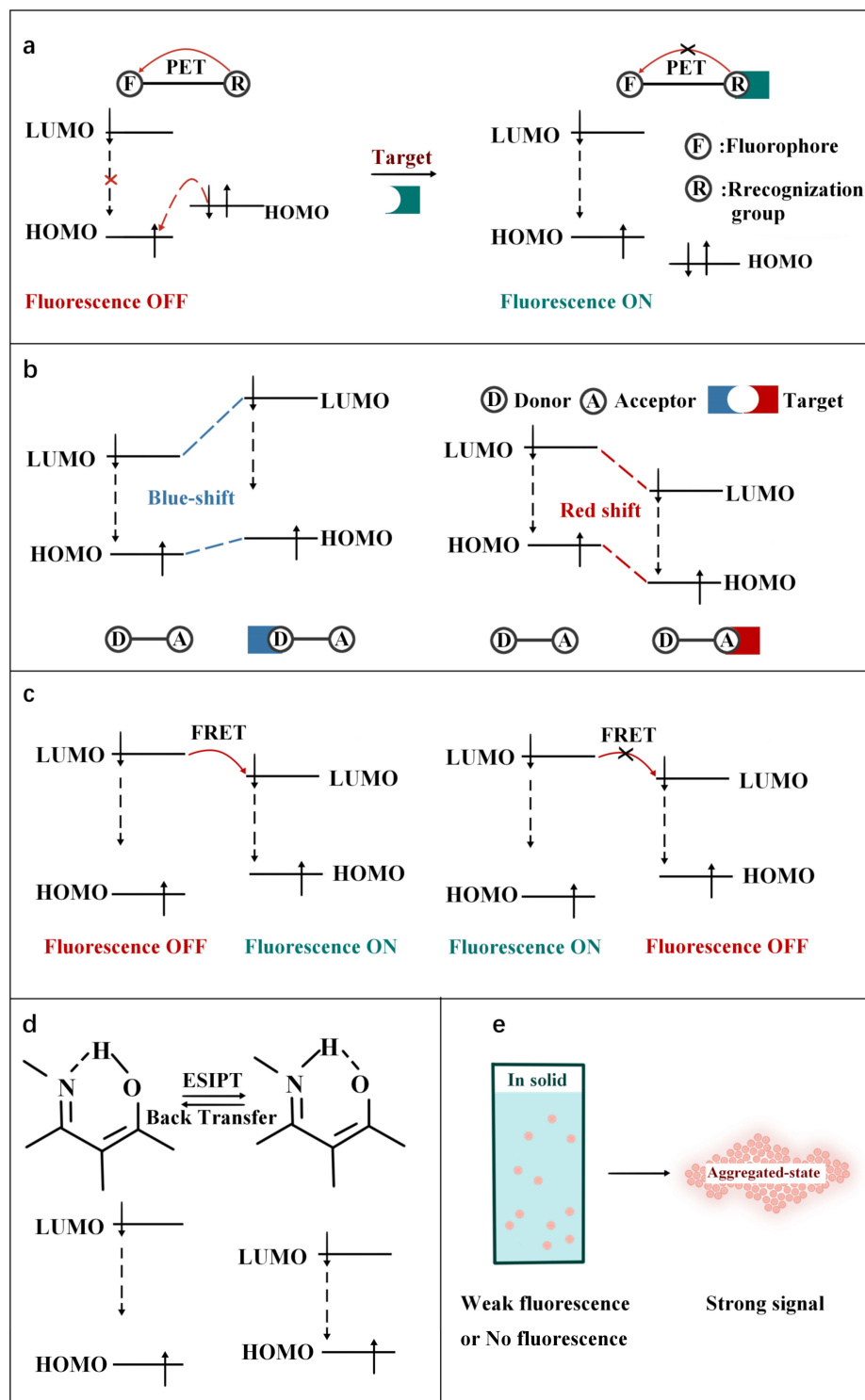


Figure 2. Schematic illustration of the principles of (a) PET, (b) ICT, (c) FRET, (d) ESIPT and (e) AIE.

Table 1. Fluorescence characteristic, recognition mechanisms, and applications of FOSMPs.

Probe	$\lambda_{ex}/\lambda_{em}$ (nm)	Mechanism	Analyte	Solvent System	Linear Detection Range	Limit of Detection (LOD)	Target	Ref.
Probe	500/525	PET	Cys	CH ₃ CN-Water-HEPES buffer	0–100 μ M	3.7×10^{-2} μ M	A375 cells	[59]
NP-S	455/551	PET	H ₂ S	PBS buffer-EtOH	30–300 μ M	0.376 μ M	Mouse liver slices	[60]
Tyro1, Tyro2	455/560	PET	Tyrosinase	Potassium phosphate buffer	-	-	B16F10 cells	[61]
NFP-G, NFP-A Naphthalimide chromophore	440/541	PET	Formaldehyde (FA)	DMSO-PBS buffer	0–30 μ M, 0–15 μ M	1.2 μ M, 0.18 μ M	HepG-2 cells	[62]
DCM- β -gal	400/502	ICT	CN ⁻	HEPES buffer -CH ₃ OH	0–15 μ M	0.066 μ M	HepG2 cells	[63]
DCDHF-Glu	535/685	ICT	β -galactosidase (β -gal)	PBS buffer-DMSO	0–12 U/L	0.17 U/L	293T cells	[64]
SHC	510/613	ICT	γ -Glutamyl-transpeptidase (GGT)	PBS buffer	0–40 U/L	0.0379 U/L	HepG2 cells, LO2 cells	[65]
AI	370/540	ICT	hNQO1	PBS buffer	0–0.8 μ M	0.0146 μ M	HT-29 cells, MDA-MB-468 cells	[66]
P-ONOO ⁻	370/495	ICT	Hypochlorous acid (HOCl)	DMSO-PBS buffer	0–50 μ M	0.84 μ M	HeLa cells, Nude mice	[67]
SR400, SR550	365/480	ICT	ONOO ⁻	DMSO-PBS buffer	0.429–3.0 μ M	0.0104 μ M	HeLa cells	[68]
CF	400/525, 550/675	FRET	H ₂ S	PBS buffer	-	-	HEK293 cells	[69]
FIP-1	415/517	FRET	HNO	PBS buffer	0–100 μ M	1.4 μ M	HeLa cells	[70]
PNCy3Cy5	515/556	FRET	Fe(II)	HEPES buffer	-	-	HEK293 cells, MDAMB-231 cells	[71]
FTR- β gal PPA	530/660	FRET	ONOO ⁻	Phosphate buffer-DMF	0–0.7 μ M	6.5×10^{-4} μ M	RAW264.7	[72]
	450/540	FRET	β -gal	PBS buffer-EtOH	0–5 U/L	4.11×10^{-8} U/L	Hek293 cells	[73]
	400/511	ESIPT	Palladium	CH ₃ CN-PBS buffer	0–180 μ M	0.028 μ M	A549 cells	[74]
Py-GSH	488/545	ESIPT	GGT	PBS buffer	1–30 U/L	1×10^{-2} U/L	SKOV3 cells, HOSEpiC cells, Tumor-bearing mice, Human specimens	[75]
NIR-TS	550/836	ESIPT	SO ₂	Water	0.5–40 μ M	0.067 μ M	HeLa cells, Mice	[76]
TPE-Gal	344/512	AIE	β -gal	PBS buffer	8×10^{-4} – 4.8×10^{-3} U/L	3.3×10^{-4} U/L	HeLa cells, OVCAR-3 cells	[77]
TT	320/ 440–550	AIE	H ₂ O ₂	DMSO-Water	-	-	RAW264.7 cells, HLF cells	[78]
QP-DNP	482/582	AIE	Hydrazine	DMSO-HEPES buffer	0–0.8 μ M	0.055 μ M	HeLa cells, Kunming mouse	[79]
AIE-Lyso-1 Probe 1	356/532	AIE/ESIPT	Esterase	DMSO-Water	100–500 U/L	2.4 U/L	MCF-7 cells	[80]
	314/446	PET/ICT	Cys	PBS buffer	0.2–2.0 μ M	1.4×10^{-3} μ M	HeLa cells	[81]
NCQ	423/490, 544 423/490423/ 490, 624	Triple-emission	Cys/Hcy, GSH/H ₂ S, thiopheno(PhSH)	PBS buffer-acetonitrile	0–10 μ M/10 μ M, 0–6 μ M/8 μ M, 0–70 μ M	0.57 μ M/0.65 μ M, 0.49 μ M/0.52 μ M, 0.34 μ M	HeLa cells	[82]

2.1. PET FOSMPs

The mechanism of PET is displayed in Figure 2a. The excited electrons on the LUMO orbital of the fluorophore cannot normally transition to its HOMO orbital when the HOMO orbital or LUMO orbital of the recognition group is between the HOMO and LUMO orbitals of fluorophore. As a result, the fluorescence of fluorophore is quenched. When binding to the target, the HOMO and LUMO orbitals of recognition group changes so that the excited electrons on the LUMO orbit of the fluorophore can normally transition to its HOMO orbital, which cuts off the PET and recovers the fluorescence emission of fluorophore [83]. Herein, several typical PET FOSMPs are introduced [59–62]. For instance, Fan et al. [59] reported a PET-based strategy for Cys detection (Figure 3a). The addition of Cys turned on the PET, and the fluorescence intensity of the probe was linearly correlated with the concentration of Cys. When 250 μ M of Cys was added, the fluorescence intensity was almost completely quenched, with a decrease of approximately 20-fold as compared with that of the free probe. Due to its low toxicity and high membrane permeability, this probe was successfully used for bioimaging (Figure 3b).

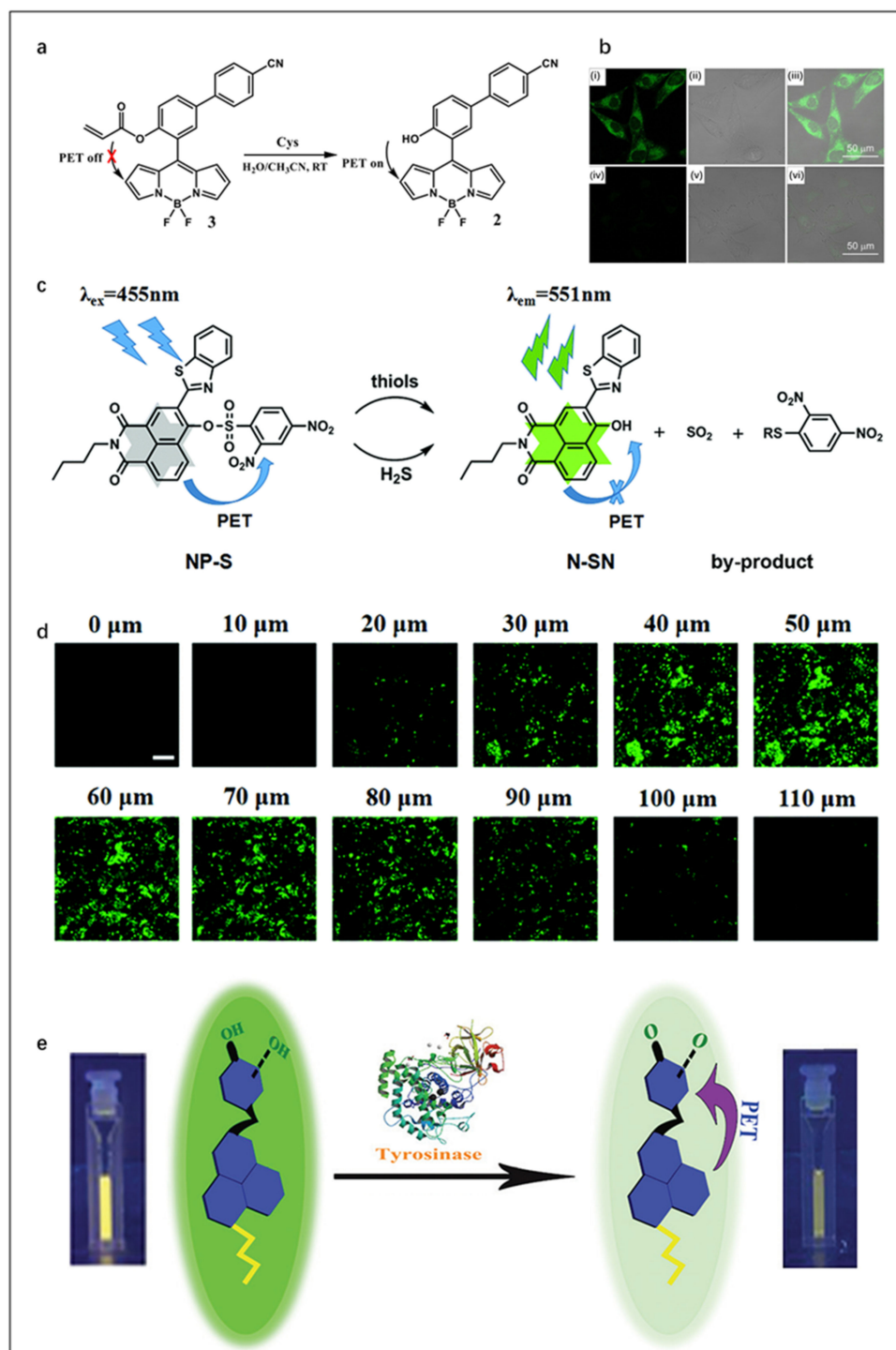


Figure 3. (a) The concept of a probe for Cys detection. (b) Confocal microscopy images of Cys detection in live A375 cells using probe. (i) Cells incubated with probe (20 μ M) for 30 min at 37 $^{\circ}$ C, (ii) bright field of (i), (iii) merge of (i,ii), (iv) probe-treated A375 cells further incubated with Cys (1 mM) for 30 min, (v) bright field of (iv), (vi) merge of (iv,v). Reproduced with permission from Ref. [59], copyright 2016, Elsevier B.V. (c) The chemical structures and the sensing mechanism of the NP-S for detecting thiols and H₂S. (d) TP imaging for mouse liver slices (Scale bar: 200 mM). Reproduced with permission from Ref. [60], copyright 2022, Royal Society of Chemistry. (e) Schematic illustration of the detection principle of tyrosinase. Reproduced with permission from Ref. [61], copyright 2020, Royal Society of Chemistry.

Xu et al. [60] synthesized a fluorescent probe named NP-S, with 2,4-dinitrobenzenesulfonyl (DNBS) as the recognition group and naphthalimide platform as the fluorophore (Figure 3c). By combining high resolution with strong tissue penetrating two-photon (TP) imaging technology, NP-S realizes high-precision detection of thiol and H₂S in vivo. The TP imaging results of mouse liver slices showed that NP-S had good tissue imaging performance (Figure 3d).

In order to realize rapid detection at a nanomolar level, Kumar et al. [61] designed a fast fluorescence probe with good photostability and pH resistance for tyrosinase detection, which can detect tyrosinase as low as 2 nM immediately after the addition of tyrosinase (Figure 3e). This probe can achieve a two-fold decrease in fluorescence intensity within 5 min. The confocal images of B16F10 cells treated with probe tyro1 demonstrated the effectiveness of the probe in detecting tyrosinase in living cells. Moreover, its fast fluorescence kinetics also has guiding significance in screening the application of tyrosinase inhibitors.

PET-based fluorescent probes have high sensitivity. However, the false positive signals generated by the combination of protons with electron-rich recognition groups in the biological environment is still a challenge in designing a PET-based fluorescent probe suitable for a wide pH range.

2.2. ICT FOSMPs

As depicted in Figure 2b, the mechanism of ICT is the change of HOMO and LUMO energy gaps of excited fluorophores caused by intramolecular charge transfer. Typically, a pair of electron donor and acceptor are connected by spacer inside the molecule. When the fluorophore molecule is exposed to the target, the degree of charge transfer changes, resulting in a “turn-on” effect response of fluorescence or a shift in wavelength [84]. Up to now, some FOSMPs based on ICT mechanism have been designed [63–68]. For example, Xiong et al. [63] designed an ICT-based probe for CN⁻ detection. The CN⁻ nucleophilic addition at the polarized C=N bond of the probe blocked the ICT process and turned on the fluorescence response, resulting in enhanced fluorescence of the green channel and blue shift of the UV-visible spectrum (603 nm to 440 nm) (Figure 4a). The probe proved to be capable of visualizing imaging in HepG2 cells.

β-gal is an important biomarker of aging and primary ovarian cancer [85]. Gu et al. [64] reported an in vivo NIR probe targeting β-gal and DCM-βgal, which achieved real-time in vivo 3D imaging of β-gal for the first time. In the presence of β-gal, the sugar portion of DCM-βgal was cleaved, thereby turning on the NIR fluorescence response (Figure 4b). This probe enabled accurate detection of β-gal with a fluorescence plateau lasting 35 min. The intensity of the emission spectrum at 685 nm increased linearly with the increase of the concentration of β-gal in the range of 0–12 U mL⁻¹, and the LOD was 1.7 × 10⁻⁴ U mL⁻¹. Human embryonic kidney cells (293T cells) were selected as a model cell line to achieve β-gal overexpression by gene transfection and to obtain quantitative ratio imaging of endogenous β-Gal activity. In addition, an IVIS spectral CT imaging system was used to obtain real-time, high-resolution 3D fluorescence images in tumor-bearing mice (Figure 4c). The fluorescence could be observed within 5 min of injection.

Shi et al. [67] synthesized a new type of HOCl fluorescent probe named AI with anisaldehyde as the donor and dicyanoisophorone as the acceptor. In the presence of HOCl, the intramolecular electrotraction group changed from the CN group to the ketone group with a lower electronegativity (Figure 4d), causing the blue shift of absorption and emission wavelength. In addition, AI can also be used to detect endogenous and exogenous HOCl acid in HeLa cells. Based on the results of cell experiments, the practicability of artificial intelligence in vivo imaging was further performed, and a strong fluorescence signal was observed by subcutaneous injection in mice.

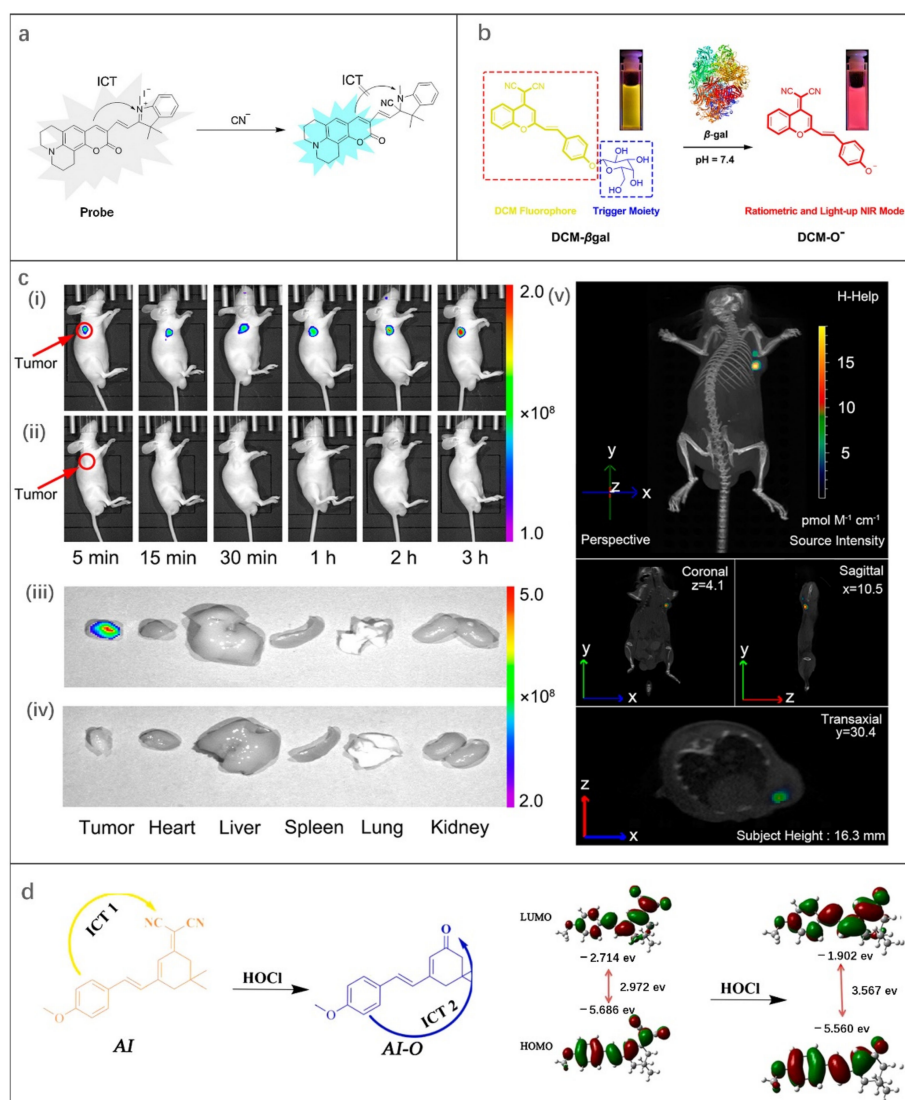


Figure 4. (a) The ICT mechanism of the probe. Reproduced with permission from Ref. [63], copyright 2015, Elsevier B.V. (b) The ICT mechanism of DCM-βgal. (c) (i,ii) In vivo imaging of β-gal activity in tumor-bearing nude mice after tumor injection, (iii,iv) fluorescence images of the main internal organs after anatomy, (v) three-dimensional in vivo imaging of β-gal activity in tumor-bearing nude mice after tumor injection of DCM-βgal for 3 h. (i,iii,v) Avidin-β-gal (100 μg) in PBS was intravenously injected into LoVo-implanted mice, and after 18 h DCM-βgal was then injected into the mice. (ii,iv) Tumor-bearing mice were not pretreated with avidin-β-gal before injection of DCM-βgal acting as the control. Reproduced with permission from Ref. [64], copyright 2022, American Chemical Society. (d) Theoretical calculation of HOMO/LUMO energy gaps of AI and AIO. Reproduced with permission from Ref. [67], copyright 2020, Elsevier B.V.

Fluorescent probes based on the ICT mechanism is widely used in the fields of bioimaging and detecting due to its simple principle [86–88]. However, if the electron donor binds to the electron-withdrawing targets (EWTs), the electron transfer of the ICT can be suppressed and the fluorescence is thus quenched [89].

2.3. FRET FOSMPs

A FRET system consists of donors and acceptors. The phenomenon of energy transfer from the excited donors to the ground state acceptors in a limited distance (10–100 Å) is called FRET. (Figure 2c). FRET can be turned on or off by changing the structure of the acceptors or the distance between the donors and the acceptors [90].

In recent years, significant progress has been made in the design of FOSMPs based on FRET mechanism [69–73]. Many FRET-based FOSMPs have been prepared and successfully used in the analytical chemistry field. Typically, Wei et al. [69] designed two ratiometric fluorescent probes (SR400 and SR550) using azido groups as reaction groups for detection of H_2S in live cells, as shown in Figure 5a. The exposure of fluorescent probe to H_2S caused the reduction of azido groups, triggering the acceptor from the closed non-fluorescent lactone structure converted to the open fluorescent structure and turning on the fluorescence response. The fluorescence intensity of the donor was weakened while that of the acceptor can be observed. Other reactive sulfur species that cannot trigger the response of the probe demonstrated the high detection selectivity of the probe for H_2S . The designed ratiometric fluorescent probe realized the imaging of H_2S in human embryonic kidney 293 cells, which is meaningful for guiding the application of H_2S -releasing drugs.

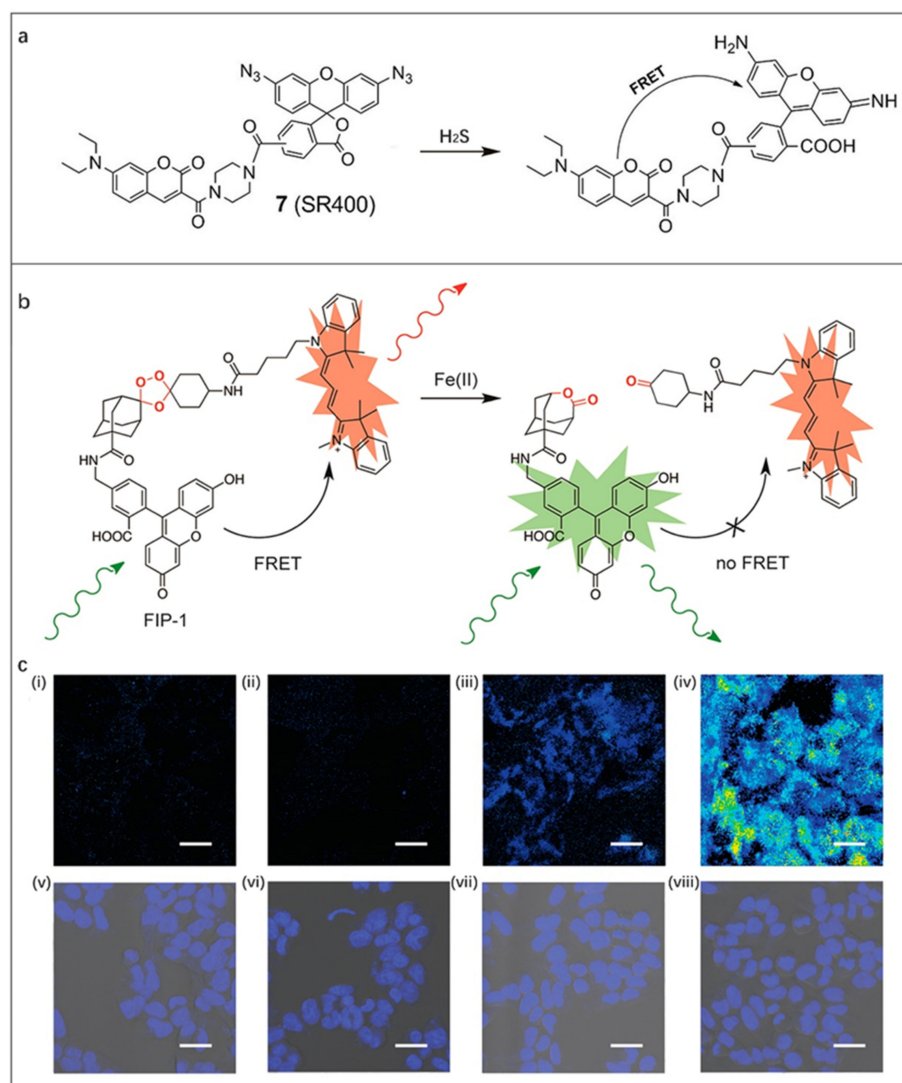


Figure 5. (a) The recognition mechanism of SR400 towards H_2S . Reproduced with permission from Ref. [69], copyright 2022, Springer Nature. (b) Design of FRET Fe(II) probe FIP-1. (c) Representative confocal microscopy images of live HEK 293T cells loaded with FIP-1. Cells treated with (i) 1 mM bathophenanthroline disulfonate for 9.5 h, (ii) 250 μM deferoxamine for 9.5 h, (iii) vehicle for 90 min, (iv) 100 μM ferrous ammonium sulfate for 90 min. (v–viii) Brightfield images of (i–iv) overlaid with Hoechst stain. Reproduced with permission from Ref. [71], copyright 2022, American Chemical Society.

Iron is the most abundant transition metal in the human body, and its level imbalance is associated with many diseases including cardiovascular diseases and cancer [91]. The intrinsic fluorescence quenching effect of Fe(II) poses a challenge to the design of fluorescent probes towards Fe(II). Based on this, Aron et al. [71] designed a reactivity-based ratiometric fluorescent probe FIP-1 to perform the imaging and detection of Fe(II) in living systems. The problems of ion interference and Fe(II)-dependent fluorescence quenching in biological environments were solved. Specifically, Fe(II) induced fluorescence response by blocking the FRET via cracking the peroxy bridging group between the donor and the acceptor inside the probe molecule (Figure 5b). Fluorescence images of live HEK 293T cells loaded with FIP-1 showed that the cells treated with Fe(II) exhibited reduced FRET effects compared with control cells, demonstrating the potential of FIP-1 in biological applications (Figure 5c).

Despite the above progress, emission spectral overlap between donor and acceptor reduces the accuracy of the fluorescence signal measurements. The fluorescence lifetime of the donor is shortened in the case of FRET [92]. Therefore, combining fluorescence lifetime imaging microscope (FLIM) with FRET can avoid the correction by using complex mathematical algorithms and provide higher temporal and spatial resolution [93]. Moreover, the coupling of FRET-FLIM with other advanced optical and mathematical technologies (such as adaptive optics [94] and unsupervised analysis [95]) may facilitate more comprehensive and precise monitoring of analytes.

2.4. ESIPT FOSMPs

ESIPT mechanism was first proposed by Weller in the 1950s [96], and it is based on proton transfer within a molecule from the relatively acidic region (e.g., hydrogen bond donor, $-\text{OH}$, $-\text{NH}_2$) to the basic region (e.g., hydrogen bond acceptor, $=\text{N}-$, $\text{C}=\text{O}$). In most cases, there is isomerization between ketones and enols in the ESIPT system, which changes the energy gap between the HOMO and LOMO orbitals of fluorophore and causes a shift in the fluorescence emission wavelength (Figure 2d). The shift in the fluorescence emission wavelength results in double fluorescence, characterized by shorter wavelengths for enol-like structures and longer wavelengths for ketone-like structures. Till now, many ESIPT-based fluorescence sensors have been designed for biocomponent analysis [74–76].

Endogenous SO_2 mediates many physiological processes, such as blood pressure and cardiac contractility, and plays an important role in maintaining redox homeostasis in organisms [97,98]. According to ESIPT mechanism, Ren et al. [76] designed a FOSMP with 2-(2'-hydroxyphenyl) benzothiazole as the fluorophore, as shown in Figure 6a. In the presence of SO_2 , the electron distribution of NIR-TS changed, resulting in a red shift of the fluorescence emission wavelength with NIR-enhanced emission at 836 nm and a large Stokes shift of 286 nm. The fluorescence signal stabilized in 10 s, and the fluorescence intensity was up to 30 folds that of the probe itself. NIR-TS has been successfully used for fluorescence imaging in Hela cells (Figure 6b) and mice (Figure 6c) with good mitochondrial targeting. This work provides a new idea for designing long wavelength ESIPT fluorescent probes.

Zhou et al. [75] developed a highly sensitive ratiometric fluorescent probe (Py-GSH) for the sensing of GGT, a biomarker of ovarian cancer (Figure 6d). The presence of GGT resulted in γ -glutamyl cleavage and subsequent intramolecular rearrangement, finally generating a new fluorescent molecule Py-GG (Figure 6e). It could be observed from the fluorescence images of the probe in human specimens that the green/red fluorescence ratio in tumor tissue was significantly higher than that in normal tissue (Figure 6f). These different ratios could provide a strong basis for the diagnosis of tumor lesions, which proved that this biodetection platform with high sensitivity and low toxicity had promising application prospects in rapid cancer diagnosis and surgical navigation during tumor resection.

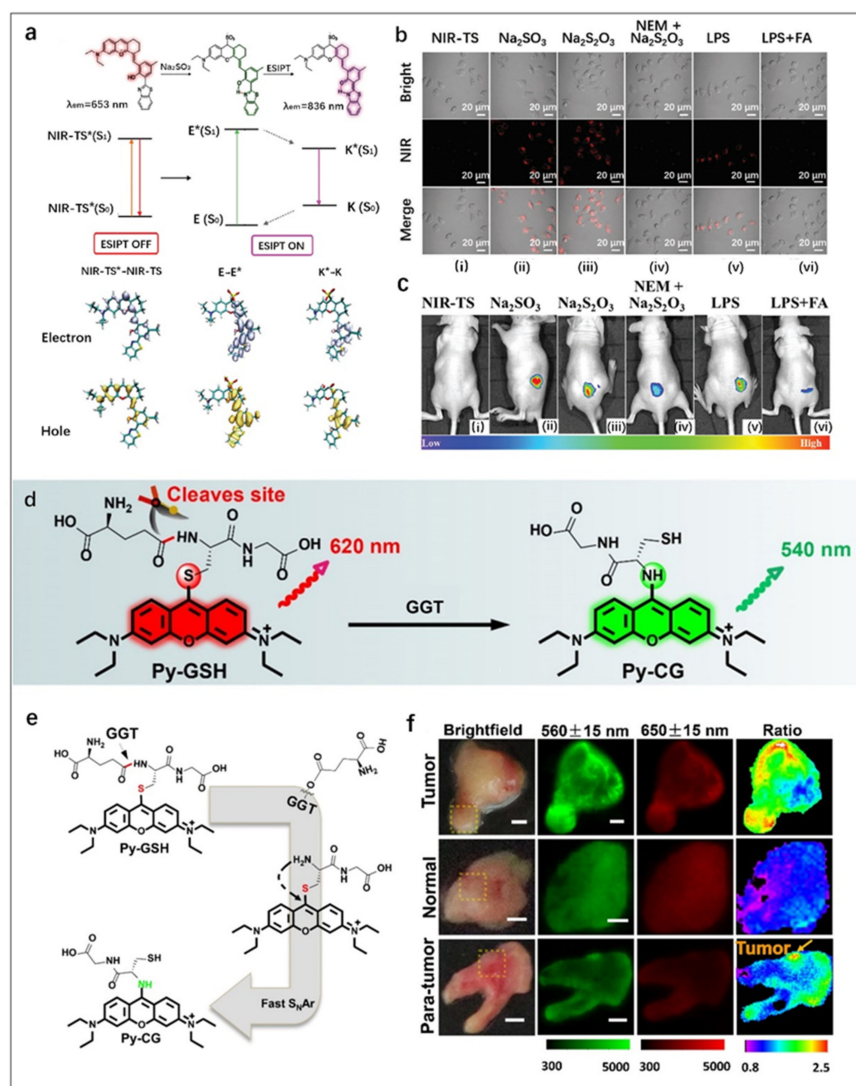


Figure 6. (a) Design of NIR-TS probe for SO_2 detection. (b) NIR fluorescence imaging of SO_2 (Na_2SO_3) in HeLa cells. (i) HeLa cells were incubated with the NIR-TS probe (10 μM) for 15 min. (ii) HeLa cells were pre-treated with the NIR-TS probe and then incubated with exogenous Na_2SO_3 (50 μM) for 10 min. (iii) HeLa cells were pretreated with the NIR-TS probe (10 μM), then incubated with $Na_2S_2O_3$ (500 μM) for 30 min. (iv) NIR-TS probe-stained HeLa cells were incubated with 500 μM N-ethylmaleimide (NEM; thiol inhibitor) for 30 min, followed by $Na_2S_2O_3$ for another 30 min. (v) HeLa cells were treated with the NIR-TS probe, then incubated with 1 $\mu\text{g mL}^{-1}$ lipopolysaccharide. (vi) HeLa cells were incubated with the NIR-TS probe, then FA (200 μM) and lipopolysaccharide (1 $\mu\text{g mL}^{-1}$) were added. (c) NIR fluorescence imaging of Na_2SO_3 in mice. (i) NIR-TS probe-treated (10 μM) mice. (ii,iii,v) NIR-TS probe-treated (10 μM) mice were also injected with Na_2SO_3 , $Na_2S_2O_3$ and LPS, respectively. (iv) As a control of (iii), mice were treated with NEM, followed by $Na_2S_2O_3$ and the NIR-TS probe. (vi) As a control of (v), mice were treated with LPS, followed by FA and NIR-TS probe. Reproduced with permission from Ref. [76], copyright 2021, Royal Society of Chemistry. (d) Design of ratiometric fluorescence probe Py-GSH for GGT detection. (e) Responsive mechanism of Py-GSH to GGT. (f) Fluorescence images of the human tissues after stain with 10 μM Py-GSH saline for 10 min. In fluorescence tissue imaging, the emission channels at 560 \pm 15 nm (Green channel) and 650 \pm 15 nm (Red channel) were collected. In ratiometric imaging, the ratio of emission intensity at 560 \pm 15 nm to 650 \pm 15 nm was chosen as the detected signal. λ_{ex} = 488 nm. Scale bar: 2 mm. Reproduced with permission from Ref. [75], copyright 2022, Ivyspring International Publisher.

Among all intramolecular photophysical reactions, ESIPT has the most significant Stokes shift [99]. However, strong hydrogen-bonded solute-solvent environments can reduce ESIPT efficiency and significantly retard ESIPT kinetics due to reliance on intramolecular proton transfer [100].

2.5. AIE FOSMPs

The concept of AIE was first proposed by Benzhong Tang in 2001 [101]. Materials with AIE effect have a unique luminescence characteristic. As depicted in Figure 2e, the molecular system does not emit fluorescence or emit weak fluorescence in the solution condition due to the free rotation of the chemical bonds. However, enhanced fluorescence is generated in the aggregation state because the rotation is inhibited. This phenomenon overcomes the aggregation-caused quenching effect of traditional fluorescent materials [102]. Based on this mechanism, many fluorescent probes have been designed [77–79].

Jiang et al. [77] reported a tetrabenzy (TPE)-based fluorescent probe TPE-Gal for β -gal detection. As shown in Figure 7a, by cleaving intramolecular β -galactoside, β -gal guided the probe molecule to form a phenolic intermediate, and the intermediate will spontaneously undergo 1,6-elimination of p-quinone-methide to obtain a poorly water-soluble product 2. AIE effect occurred in the aggregated state of product 2, and the fluorescence intensity gradually increased and reached a plateau in 9 min. TPE-Gal showed very weak fluorescence emission in HeLa cells but showed strong fluorescence in OVCAR-3 cells from human ovarian cancer patients, indicating the overexpression of endogenous β -gal in tumor cells (Figure 7b). These results demonstrated the potential of TPE-Gal in cancer diagnosis.

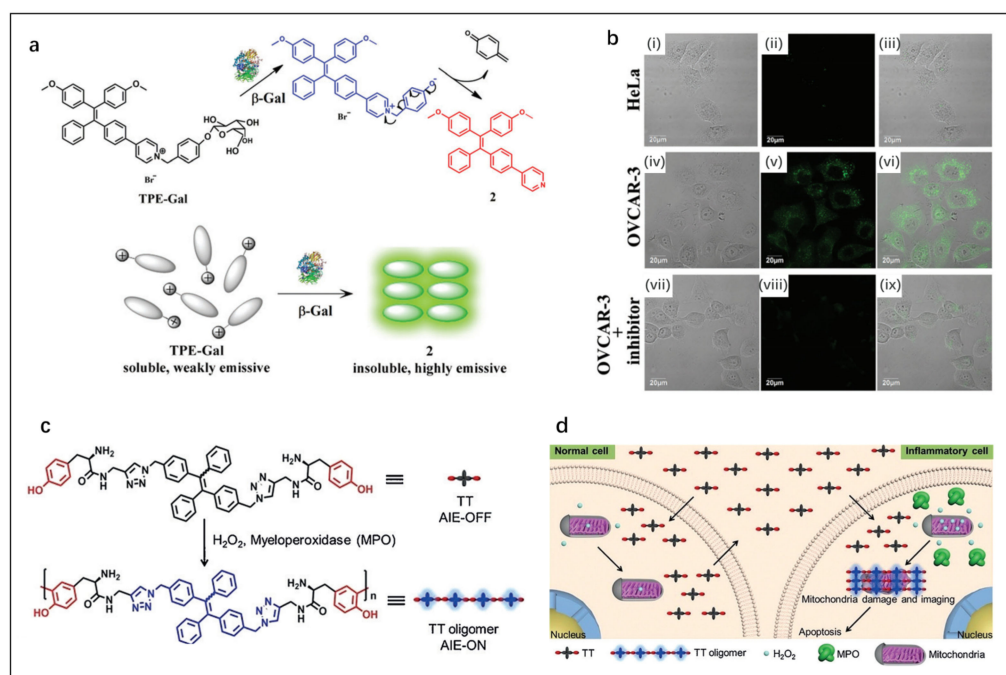


Figure 7. (a) Schematic representation of light-up sensing of β -gal. (b) Confocal fluorescence microscopy images of HeLa and OVCAR-3 cells incubated with TPE-Gal (10 mM) for 40 min: (i–iii) HeLa cells, (iv–vi) OVCAR-3 cells, and (vii–ix) OVCAR-3 cells pretreated with an inhibitor (50 mM) ($\lambda_{ex} = 405$ nm). Reproduced with permission from Ref. [77], copyright 2022, Royal Society of Chemistry. (c) Peroxidase-catalyzed oligomerization of TT in the presence of H_2O_2 . (d) Selective imaging and inhibition of inflammatory cells after incubation of co-cultured cells with TT. Reproduced with permission from Ref. [78], copyright 1999–2022, John Wiley & Sons, Inc.

Cheng et al. [78] designed a new therapeutic multifunctional AIE probe named TT. When exposed to H_2O_2 and overexpressed myeloperoxidase in inflammatory cells, TT

can crosslink into hydrophobic aggregates, activating the AIE (Figure 7c). In addition, a large number of TT aggregates induced mitochondria damage and inflammatory cell apoptosis but were harmless to normal cells (Figure 7d). Cell imaging proved that TT can distinguish inflammatory cells from normal cells and has a selective cell inhibition effect. TT is a powerful tool for accurate inflammation detection and treatment.

Because the triggering of AIE effect requires a high concentration of local molecules, reducing cytotoxicity is a design consideration. At the same time, the ubiquitous conjugated phenolic rings in AIE probes may lead to intracellular distribution and metabolic problems [103].

2.6. Multi-Mechanism FOSMPs

Compared to single sensing mechanism-based FOSMPs, multiple sensing mechanism-based FOSMPs can achieve signal amplification and diversification, which is conducive to realize the tracking of a variety of analytes and to improve the sensitivity of the detection [80–82].

Gao et al. [80] reported a fluorescent probe named AIE-Lyso-1 with “AIE + ESIPT” characteristics for in situ visualization of lysosomal esterase activity and motility (Figure 8a). The probe molecule consists of lysosome-targeted morpholine, esterase-reactive acetoxyl, and salicyladazine fluorophore. The free rotation of the probe molecule resulted in quenching of the salicyladazine fluorophore. After reacting with esterase, the acetyl group was cleaved and the product molecule 2 was generated. The formation of intramolecular hydrogen bond activated the ESIPT and AIE reactions of molecule 2 at the same time. Real-time imaging of MCF-7 cells proved that AIE-Lyso-1 could be used for in situ monitoring of lysosomal esterase activity. In addition, this probe has the advantages of no self-quenching and good luminescence in lysosomal profiling. Furthermore, this dual-mechanism sensing is conducive to the formation of a large Stokes-shifted ESIPT emission that amplifies the response signal.

Biothiols with similar molecular structures, such as Cys, Hcy, GSH, H₂S and PhSH play important roles in enzymatic catalysis, redox reactions, protein synthesis and other metabolic activities in the human body. The imbalance in the concentration levels of these substances is related to some diseases [104,105]. Therefore, it is essential to develop methods to distinguish them. Based on “ICT + PET” mechanisms, Chen et al. [81] reported a fluorescent probe for the high-sensitivity and selective differentiation of Cys from other biothiols. The maleimide group typically exhibited no or weak fluorescence due to the presence of an effective PET quenching pathway in the LUMO orbital. Upon thiol-michael addition, the above orbital was removed and PET quenching was eliminated. Meanwhile, EWTs-induced fluorescence quenching of the succinimide group at the 4-position still kept the molecule in a low fluorescence. Only Cys adducts can remove the ICT quenching by intramolecular transcyclization reaction, and more than 3000-fold fluorescence could be achieved due to the elimination of the double quenching effect (Figure 8b).

In order to achieve simultaneous tracking of Cys/Hcy, GSH/H₂S, and PhSH in living cells, Yang et al. [82] integrated two sensing groups (2, 4-dinitrobenzene (DNB) and 7-nitro-1,2,3-benzoxadiazole (NBD)) and two fluorophores into a fluorescent probe molecule (NCQ) through ether bonds, as shown in Figure 8c. After the reaction between active site 1 and Cys/Hcy, GSH/H₂S and PhSH, respectively, NBD-S-Cys/Hcy with green fluorescence and NBD-S-GSH/NBD-SH and NBD-SPh without fluorescence were obtained. Active site 2 is active towards PhSH and inert towards the other four molecules. PhSH could break the ether bonds of DNB and NBD, releasing blue-emitting coumarin 1 and then forming red-emitting TQC. The detection can be realized by monitoring the combination of three-color fluorescence signals (blue-green-red). The detection limits of NCQ for Cys, Hcy, GSH, H₂S and PhSH were 0.57, 0.65, 0.49, 0.52 and 0.34 μM, respectively.

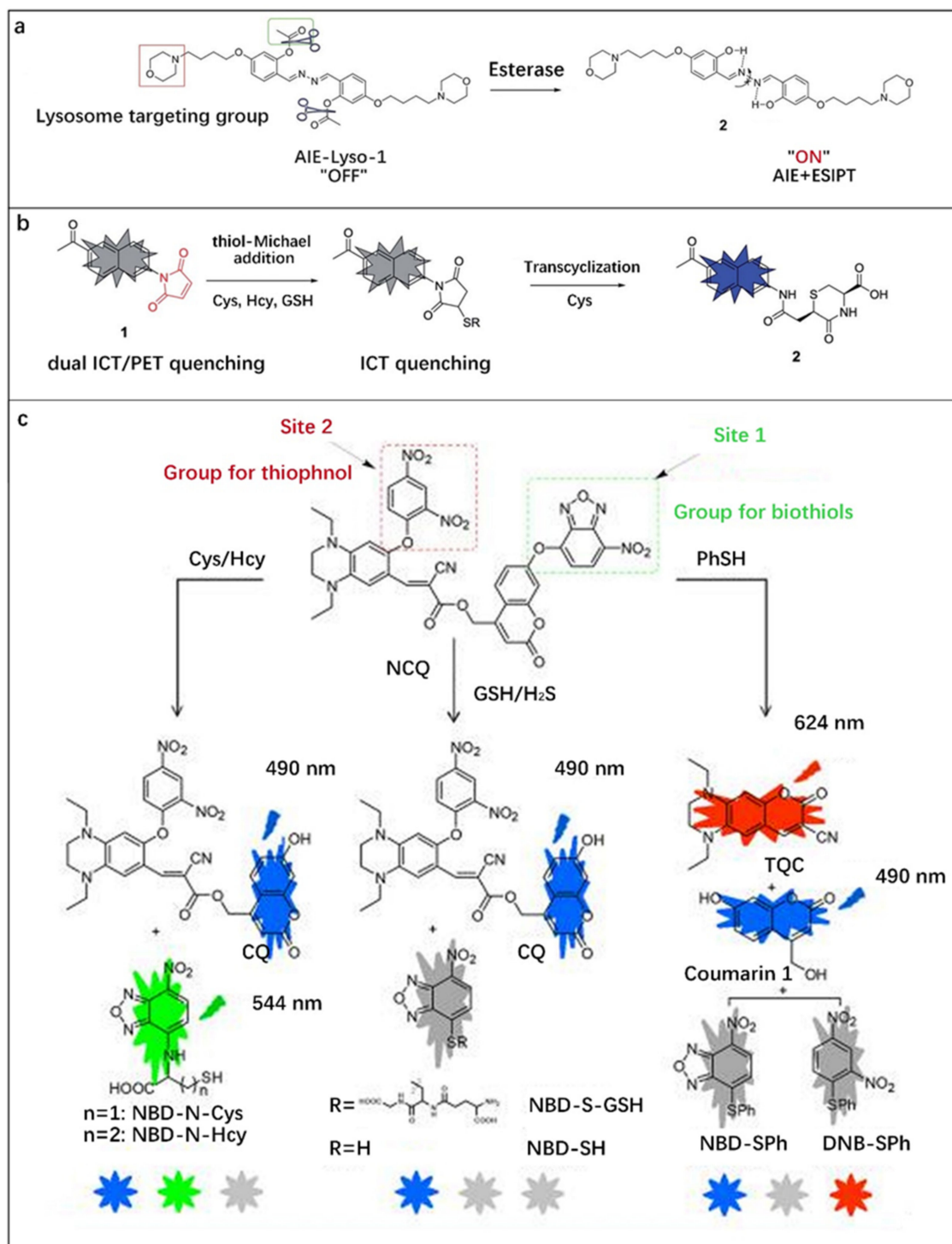


Figure 8. (a) Design of AIE-Lyso-1 for specific detection of lysosomal esterase. Reproduced with permission from Ref. [80], copyright 2014, Royal Society of Chemistry. (b) Design principle of probe 1 for selective detection of Cys. Reproduced with permission from Ref. [81], copyright 2018, Royal Society of Chemistry. (c) Sensing Mechanism of NCQ for distinguishing Cys/Hcy, GSH/H₂S and thiophenol. Reproduced with permission from Ref. [82], copyright 2022, American Chemical Society.

3. FOSMPs-Based FONPs for Bioimaging and Detection

Compared with FOSMPs, FONPs have larger surface area, better biodegradability and greater resistance to photobleaching [106,107]. FONPs-based multifunctional biodetection platforms can be constructed through drug encapsulation and surface modification of targeting groups. This section briefly describes the preparation and applications of FOSMPs-based FONPs in bioimaging and detection.

Zhang et al. [108] reported a strategy to prepare FONPs by encapsulating the fluorophore C18-R in synthetic copolymer matrices (Figure 9a). First, the copolymer aqueous solution was added to the C18-Rd THF solution under sonication. In the process of removing THF, the hydrophobic segment of the copolymer wrapped C18-R through hydrophobic interaction to form a “core-shell” structure, and finally the C18-R-PEG FONPs were obtained. CLSM images and cell uptake experiments proved that the C18-R-PEG FONPs has good biocompatibility and can be used for bioimaging.

Enhanced fluorescence emission can be obtained by loading high concentrations of fluorophores into FONPs since AIE can occur at high concentrations of fluorophores. Zhang et al. [109] prepared near-infrared emitting AIE dots with a particle size of ~20 nm and a fluorescence quantum efficiency of 20% by using the amphiphilic polymer poly(styrene co maleic anhydride) (PSMA) as the co-encapsulation matrix and a novel small-molecule fluorophore (2Z,2'Z)-3,3'-(2,5-di(piperidin-1-yl)-1,4-phenylene)bis(2-phenylacrylonitrile) (DPPBPA) as the core (Figure 9b). The final product SA dots were obtained by modifying streptavidin on its surface to achieve specific binding to target cells. SA dots have been successfully used for fluorescence imaging of MCF-7 cell line benefit from their uniform size, stable luminescence and excellent biocompatibility.

1,2-distearoyl-sn-glycero-3-phosphoethanolamine-N-(polyethylene glycol) (DSPE-PEG₂₀₀₀) is a typical package matrix that is widely used in the design of FONPs due to its good biocompatibility [110–113]. Transcription-AIE (Tat-AIE) dots prepared using DSPE-PEG₂₀₀₀ as the matrix was first reported as cell-tracing probes in 2013, showing brighter fluorescence, better fluorescence stability and cell-tracking ability than commercial quantum dot-based probes. In this work, Li et al. [111] encapsulated the fluorophore TPETPAFN by using a mixture of DSPE-PEG₂₀₀₀ and DSPE-PEG₂₀₀₀-NH₂ (Figure 10a). Then, Tat-AIE dots were obtained by coupling AIE dots with cell penetrating peptide HIV-1 Tat. TPETPAFN has poor water solubility but is easily soluble in THF solution. The fluorescence of TPETPAFN was turned on when the THF/water volume ratio was 1:1 and the fluorescence intensity increased exponentially with the increase of the ratio of water. The fluorescence intensity of TPETPAFN showed a 70-fold enhancement at a 90% water volume fraction (Figure 10b). The hydrodynamic size and quantum yield of the as-prepared NIR-emitting Tat-AIE dots were ~30 nm and 24%, respectively (Figure 10c). Compared to commercial Qtracker[®] 655, Tat-AIE dots displayed 10-fold stronger fluorescence intensity and better long-term tracing ability (Figure 10d). Tat-AIE dots could trace MCF-7 cells for 10–12 generations and trace C6 cells for 21 days in vivo (Figure 10e). This work shows the promise of FONPs as an ideal alternative to quantum dots in fluorescence imaging and non-invasive long-term cell tracing.

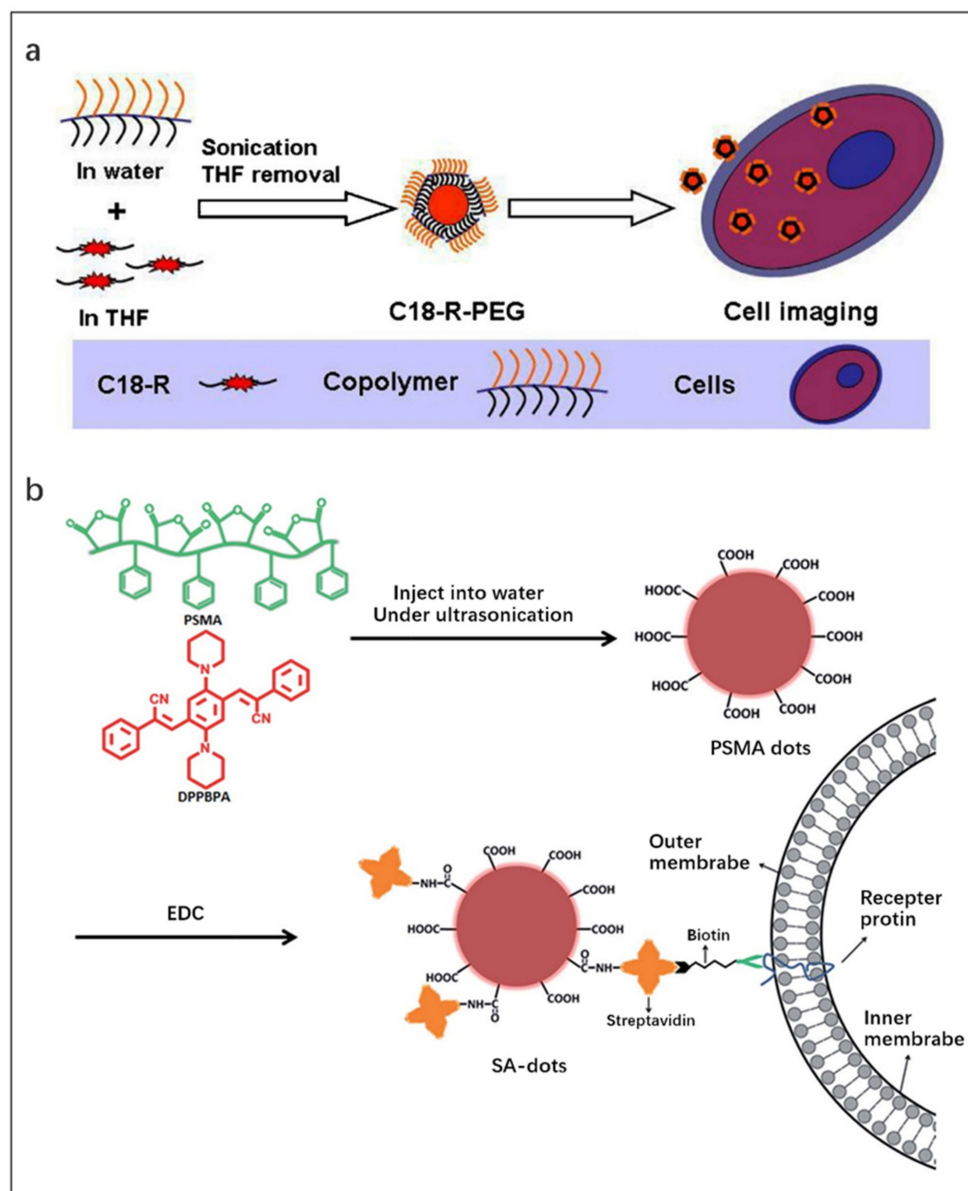


Figure 9. (a) Schematic illustration of the formation of C18-R-PEG FONPs via self-assembly of C18-R and synthetic copolymers and their utilization in cell imaging. Reproduced with permission from Ref. [108], copyright 2013, Published by Elsevier B.V. (b) Schematic illustration of the preparation of SA-dots via EDC-catalyzed coupling and their subsequent cell marking. Reproduced with permission from Ref. [109], copyright 2015, Royal Society of Chemistry.

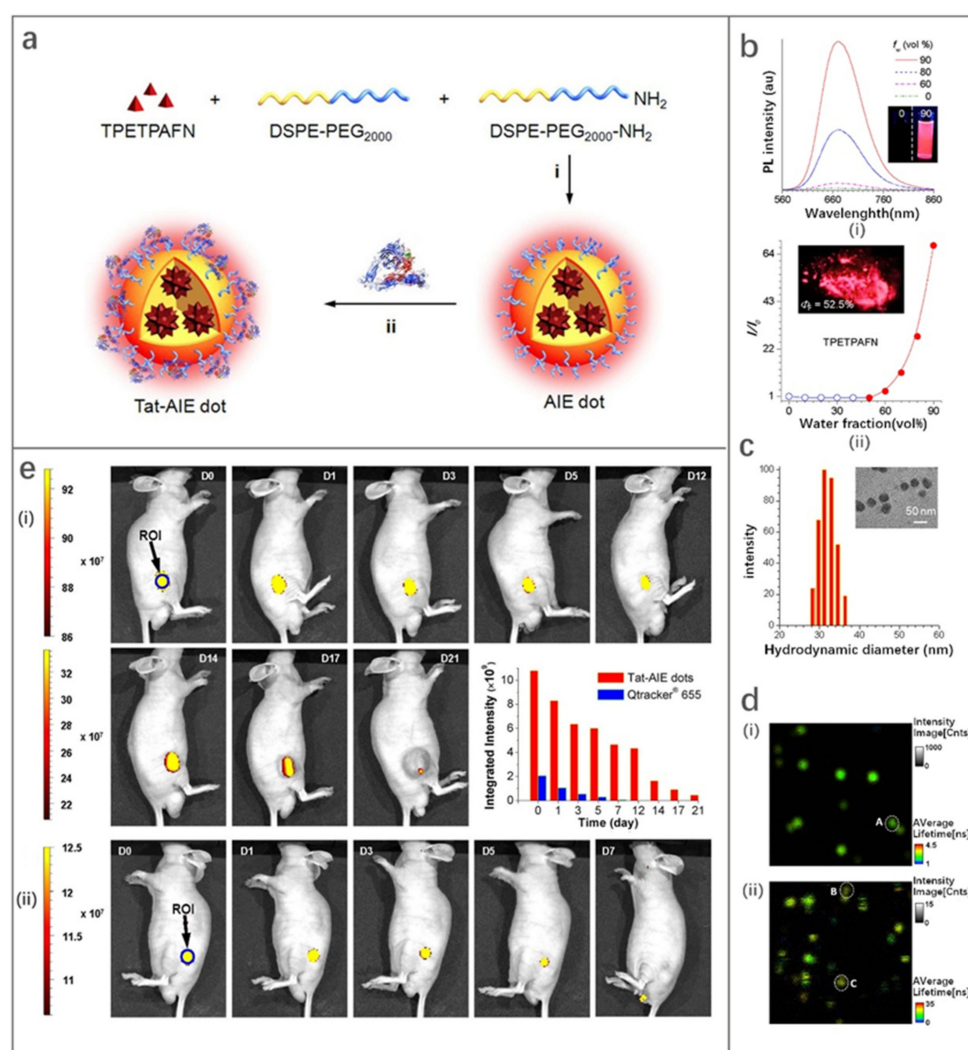


Figure 10. (a) Schematic illustration of fabrication of Tat-AIE dots. (b) (i) Photoluminescence (PL) spectra and (ii) I/I_0 intensity of TPETPAFN in THF/water mixtures with different water fractions. (c) Particle size distribution and morphology of Tat-AIE dots. (d) Fluorescence lifetime imaging (FLIM, $5 \times 5 \mu\text{m}^2$) results of (i) Tat-AIE dots and (ii) Qtracker[®] 655. (e) In vivo fluorescence imaging of tumor cells by Tat-AIE dots. (i) Representative in vivo fluorescence images of the mouse subcutaneously injected with 1×10^6 of C6 glioma cells after staining by 2 nM Tat-AIE dots. (ii) Data for Qtracker[®] 655 obtained under similar conditions. The inset in the middle panel showed the integrated PL intensities of the regions of interest (blue circles) at the tumor sites from the corresponding images. Reproduced with permission from Ref. [111], copyright 2022, Springer Nature.

4. Conclusions and Perspectives

This review has summarized the applications of FOSMPs in bioimaging and detection relying on different mechanisms, including PET, ICT, AIE, FRET, ESIP and their combinations. The performance of these sensing modalities was also discussed. FOSMPs based on different detection mechanisms show the advantages and deficiencies in fluorescent performance, sensitivity, accuracy, adaptability and biological toxicity. Compared to single-mechanism-based detection mode, multi-mechanism-based biosensing displays diversified fluorescence signals, leading to more precise detection. Furthermore, the synthesis and biological applications of FONPs designed with FOSMPs as fluorophores were also introduced. In short, FOSMPs have been widely used in the field of bioanalysis, greatly facilitating the diagnosis and treatment of various diseases.

Nevertheless, some improvements are still needed to facilitate the practical application of FOSMPs. First, the properties of FOSMPs are easily affected by the detection environment, which hinders their application in a complex physiological environment. The design of FOSMPs with a large Stokes shift, high fluorescence intensity, good fluorescence stability and low toxicity is an ongoing effort. In addition, many FOSMPs are designed based on irreversible chemical reactions. FOSMPs prepared by reversible chemical reaction should be further investigated to realize reversible and dynamic real-time detection of cell state. Furthermore, the design of FOSMPs with targeted delivery and signal amplification functions is also a promising direction in the future. Second, super-resolution microscope technology has been booming in recent years [114], and it provides more application scenarios for FOSMPs. FOSMPs with high quantum yield, long fluorescence life and multiple reaction sites are required to achieve resolution imaging at the molecular level and to monitor the dynamic changes of subcellular organelles by this novel technology. Third, the exploration of multi-mechanism detection modes should be strengthened to improve the sensitivity and reliability of bioimaging and detection. The combination of multiple mechanisms aims to construct sensors with large signal-to-noise ratios and strong fluorescent signals and can simultaneously trace multiple analytes. Fourth, matrices with good biocompatibility and stability and active surface groups for modifying FOSMPs should be explored to obtain multifunctional and practical FOSMPs. It is expected that the continuous development of FOSMPs and biosensing strategies based on FOSMPs will greatly facilitate the advancement of disease diagnosis techniques.

Author Contributions: Conceptualization, J.Z., Z.S. and Y.J.; validation, Y.Y., F.G. and Y.W.; investigation, Y.Y. and Z.S.; resources, H.L.; writing—original draft preparation, Y.Y.; writing—review and editing, J.Z., Z.S. and Y.J.; funding acquisition, H.L. and Y.J. All authors have read and agreed to the published version of the manuscript.

Funding: The authors acknowledge financial support from the National Natural Science Foundation of China (grant nos. 52101287 and U1806219). This work is also supported by the Special Funding in the Project of the Taishan Scholar Construction Engineering and the program of Jinan Science and Technology Bureau (grant no. 2020GXRC019) as well as the new material demonstration platform construction project from the Ministry of Industry and Information Technology (grant no. 2020-370104-34-03-043952-01-11). The Special Funding also supports this work in the Project of the Qilu Young Scholar Program of Shandong University.

Institutional Review Board Statement: Not applicable.

Informed Consent Statement: Not applicable.

Data Availability Statement: Not applicable.

Conflicts of Interest: The authors declare no conflict of interest.

References

1. Hao, J.; Yan, B. A water-stable lanthanide-functionalized MOF as a highly selective and sensitive fluorescent probe for Cd²⁺. *Chem. Commun.* **2015**, *51*, 7737–7740. [[CrossRef](#)] [[PubMed](#)]
2. Donia, M.S.; Fischbach, M.A. Small molecules from the human microbiota. *Science* **2015**, *349*, 1254766. [[CrossRef](#)]
3. Fukuto, J.M.; Carrington, S.J.; Tantillo, D.J.; Harrison, J.G.; Ignarro, L.J.; Freeman, B.A.; Chen, A.; Wink, D.A. Small Molecule Signaling Agents: The Integrated Chemistry and Biochemistry of Nitrogen Oxides, Oxides of Carbon, Dioxygen, Hydrogen Sulfide, and Their Derived Species. *Chem. Res. Toxicol.* **2012**, *25*, 769–793. [[CrossRef](#)] [[PubMed](#)]
4. Griending, K.K.; Touyz, R.M.; Zweier, J.L.; Dikalov, S.; Chilian, W.; Chen, Y.; Harrison, D.G.; Bhatnagar, A.; Amer, H.A.C.B. Measurement of Reactive Oxygen Species, Reactive Nitrogen Species, and Redox-Dependent Signaling in the Cardiovascular System: A Scientific Statement From the American Heart Association. *Circ. Res.* **2016**, *119*, E39–E75. [[CrossRef](#)] [[PubMed](#)]
5. Jiao, X.; Li, Y.; Niu, J.; Xie, X.; Wang, X.; Tang, B. Small-Molecule Fluorescent Probes for Imaging and Detection of Reactive Oxygen, Nitrogen, and Sulfur Species in Biological Systems. *Anal. Chem.* **2018**, *90*, 533–555. [[CrossRef](#)]
6. Kalyanaraman, B. Teaching the basics of redox biology to medical and graduate students: Oxidants, antioxidants and disease mechanisms. *Redox Biol.* **2013**, *1*, 244–257. [[CrossRef](#)]

7. Figueira, T.R.; Barros, M.H.; Camargo, A.A.; Castilho, R.F.; Ferreira, J.C.B.; Kowaltowski, A.J.; Sluse, F.E.; Souza-Pinto, N.C.; Vercesi, A.E. Mitochondria as a Source of Reactive Oxygen and Nitrogen Species: From Molecular Mechanisms to Human Health. *Antioxid. Redox Sign.* **2013**, *18*, 2029–2074. [[CrossRef](#)]
8. Fransen, M.; Nordgren, M.; Wang, B.; Apanasets, O. Role of peroxisomes in ROS/RNS-metabolism: Implications for human disease. *Bba.-Mol. Basis Dis.* **2012**, *1822*, 1363–1373. [[CrossRef](#)]
9. Mehta, V.N.; Desai, M.L.; Basu, H.; Kumar Singhal, R.; Kailasa, S.K. Recent developments on fluorescent hybrid nanomaterials for metal ions sensing and bioimaging applications: A review. *J. Mol. Liq.* **2021**, *333*, 115950. [[CrossRef](#)]
10. Huang, J.; Jones, A.; Waite, T.D.; Chen, Y.; Huang, X.; Rosso, K.M.; Kappler, A.; Mansor, M.; Tratnyek, P.G.; Zhang, H. Fe(II) Redox Chemistry in the Environment. *Chem. Rev.* **2021**, *121*, 8161–8233. [[CrossRef](#)] [[PubMed](#)]
11. Kim, S.; Noh, J.Y.; Kim, K.Y.; Kim, J.H.; Kang, H.K.; Nam, S.; Kim, S.H.; Park, S.; Kim, C.; Kim, J. Salicylimine-Based Fluorescent Chemosensor for Aluminum Ions and Application to Bioimaging. *Inorg. Chem.* **2012**, *51*, 3597–3602. [[CrossRef](#)]
12. Kumar, A.; Palfrey, H.A.; Pathak, R.; Kadowitz, P.J.; Gettys, T.W.; Murthy, S.N. The metabolism and significance of homocysteine in nutrition and health. *Nutr. Metab.* **2017**, *14*, 78. [[CrossRef](#)] [[PubMed](#)]
13. Skovierova, H.; Vidomanova, E.; Mahmood, S.; Sopkova, J.; Drgova, A.; Cervenova, T.; Halasova, E.; Lehotsky, J. The Molecular and Cellular Effect of Homocysteine Metabolism Imbalance on Human Health. *Int. J. Mol. Sci.* **2016**, *17*, 1733. [[CrossRef](#)]
14. Poole, L.B. The basics of thiols and cysteines in redox biology and chemistry. *Free Radical Bio. Med.* **2015**, *80*, 148–157. [[CrossRef](#)]
15. Dao, N.V.; Ercole, F.; Urquhart, M.C.; Kaminskas, L.M.; Nowell, C.J.; Davis, T.P.; Sloan, E.K.; Whittaker, M.R.; Quinn, J.F. Trisulfide linked cholesteryl PEG conjugate attenuates intracellular ROS and collagen-1 production in a breast cancer co-culture model. *Biomater. Sci. UK* **2021**, *9*, 835–846. [[CrossRef](#)] [[PubMed](#)]
16. Chen, X.; Wang, F.; Hyun, J.Y.; Wei, T.; Qiang, J.; Ren, X.; Shin, I.; Yoon, J. Recent progress in the development of fluorescent, luminescent and colorimetric probes for detection of reactive oxygen and nitrogen species. *Chem. Soc. Rev.* **2016**, *45*, 2976–3016. [[CrossRef](#)] [[PubMed](#)]
17. Graves, D.B. The emerging role of reactive oxygen and nitrogen species in redox biology and some implications for plasma applications to medicine and biology. *J. Phys. D Appl. Phys.* **2012**, *45*, 263001. [[CrossRef](#)]
18. Van-Nghia, N.; Ha, J.; Cho, M.; Li, H.; Swamy, K.M.K.; Yoon, J. Recent developments of BODIPY-based colorimetric and fluorescent probes for the detection of reactive oxygen/nitrogen species and cancer diagnosis. *Coordin. Chem. Rev.* **2021**, *439*, 213936.
19. Ogawa, M.; Takakura, H. In Vivo Molecular Imaging for Biomedical Analysis and Therapies. *Anal. Sci.* **2018**, *34*, 273–281. [[CrossRef](#)]
20. Peng, F. Recent Advances in Cancer Imaging with (CuCl₂)-Cu-64 PET/CT. *Nucl. Med. Mol. Imaging.* **2022**, *56*, 80–85. [[CrossRef](#)]
21. Yan, Y.; Wang, H.; Zhao, Y. Radiolabeled peptide probe for tumor imaging. *Chinese Chem. Lett.* **2022**, *33*, 3361–3370. [[CrossRef](#)]
22. Seetharam Bhat, K.R.; Samavedi, S.; Moschovas, M.C.; Onol, F.F.; Roof, S.; Rogers, T.; Patel, V.R.; Sivaraman, A. Magnetic resonance imaging-guided prostate biopsy—A review of literature. *Asian J. Urol.* **2021**, *8*, 105–116. [[CrossRef](#)] [[PubMed](#)]
23. Kitada, N.; Maki, S.; Kim, S. Visible Light Bioluminescence Imaging Platform for Animal Cell Imaging. *Methods Mol. Biol.* **2022**, *2524*, 37–51.
24. Komatsu, H.; Kobayashi, E.; Gonzalez, N.; Rawson, J.; Ortiz, J.; Donohue, C.; Ku, H.T.; Kandeel, F.; Mullen, Y. Critical Considerations in Bioluminescence Imaging of Transplanted Islets Dynamic Signal Change in Early Posttransplant Phase and Signal Absorption by Tissues. *Pancreas* **2022**, *51*, 234–242. [[CrossRef](#)]
25. Sato, K. Bioluminescence Imaging for Evaluation of Antitumor Effect In Vitro and In Vivo in Mice Xenografted Tumor Models. *Methods Mol. Biol.* **2022**, *2524*, 307–315. [[PubMed](#)]
26. Pan, X.; Gao, A.; Lin, Z. Fluorescence imaging of tumor immune contexture in immune checkpoint blockade therapy. *Int. Immunopharmacol.* **2022**, *106*, 108617. [[CrossRef](#)] [[PubMed](#)]
27. Wu, X.; Li, H.; Lee, E.; Yoon, J. Sensors for In Situ Real-Time Fluorescence Imaging of Enzymes. *Chem* **2020**, *6*, 2893–2901. [[CrossRef](#)]
28. Zhu, H.; Hamachi, I. Fluorescence imaging of drug target proteins using chemical probes. *J. Pharm. Sci.* **2020**, *10*, 426–433. [[CrossRef](#)]
29. van Manen, L.; Handgraaf, H.J.M.; Diana, M.; Dijkstra, J.; Ishizawa, T.; Vahrmeijer, A.L.; Mieog, J.S.D. A practical guide for the use of indocyanine green and methylene blue in fluorescence-guided abdominal surgery. *J. Surg. Oncol.* **2018**, *118*, 283–300. [[CrossRef](#)] [[PubMed](#)]
30. Wang, J.; Li, C.; Jiang, G. Progress in Fluorescent Probes for Aminopeptidase N. *Chem. Eur. J.* **2018**, *81*, 972–980.
31. Xu, Y.; Liu, R.; Xu, K.; Dai, Z. Fluorescent Probes for Intraoperative Navigation. *Prog. Chem.* **2021**, *33*, 52–65.
32. Yagishita, A.; Ueno, T.; Tsuchihara, K.; Urano, Y. Amino BODIPY-Based Blue Fluorescent Probes for Aldehyde Dehydrogenase 1-Expressing Cells. *Bioconjugate Chem.* **2021**, *32*, 234–238. [[CrossRef](#)] [[PubMed](#)]
33. Han, H.; Zhong, Y.; He, C.; Fu, L.; Huang, Q.; Kuang, Y.; Yi, X.; Zeng, W.; Zhong, H.; Yang, M. Recent advances in organic fluorescent probes for tumor related enzyme detection. *Dyes Pigm.* **2022**, *204*, 110386. [[CrossRef](#)]
34. Pak, Y.L.; Swamy, K.; Yoon, J. Recent Progress in Fluorescent Imaging Probes. *Sensors* **2015**, *15*, 24374–24396. [[CrossRef](#)] [[PubMed](#)]
35. Shaya, J.; Corridon, P.R.; Al-Omari, B.; Aoudi, A.; Shunnar, A.; Mohideen, M.I.H.; Qurashi, A.; Michel, B.Y.; Burger, A. Design, photophysical properties, and applications of fluorene-based fluorophores in two-photon fluorescence bioimaging: A review. *J. Photoch. Photobio. C.* **2022**, *52*, 100529. [[CrossRef](#)]

36. Terai, T.; Nagano, T. Fluorescent probes for bioimaging applications. *Curr. Opin. Chem. Biol.* **2008**, *12*, 515–521. [[CrossRef](#)] [[PubMed](#)]
37. Balleza, E.; Kim, J.M.; Cluzel, P. Systematic characterization of maturation time of fluorescent proteins in living cells. *Nat. Methods* **2018**, *15*, 47. [[CrossRef](#)]
38. Han, Y.; Wang, X.; Li, S. Biocompatible Europium Doped Hydroxyapatite Nanoparticles as a Biological Fluorescent Probe. *Curr. Nanosci.* **2010**, *6*, 178–183. [[CrossRef](#)]
39. Shore, A. A review on fluorescent inorganic nanoparticles for optical sensing applications (vol 6, pg 21624, 2016). *RSC Adv.* **2019**, *9*, 16565. [[CrossRef](#)]
40. Wu, C.; Chiu, D.T. Highly Fluorescent Semiconducting Polymer Dots for Biology and Medicine. *Angew. Chem. Int. Edit.* **2013**, *52*, 3086–3109. [[CrossRef](#)]
41. Zhang, J.; Huang, Y.; Wang, D.; Pollard, A.C.; Chen, Z.G.; Egap, E. Triblock near-infrared fluorescent polymer semiconductor nanoparticles for targeted imaging. *J. Mater. Chem. C.* **2017**, *5*, 5685–5692. [[CrossRef](#)]
42. Chan, J.; Dodani, S.C.; Chang, C.J. Reaction-based small-molecule fluorescent probes for chemoselective bioimaging. *Nat. Chem.* **2012**, *4*, 973–984. [[CrossRef](#)]
43. Gu, B.; Zhang, Q. Recent Advances on Functionalized Upconversion Nanoparticles for Detection of Small Molecules and Ions in Biosystems. *Adv. Sci.* **2018**, *5*, 1700609. [[CrossRef](#)] [[PubMed](#)]
44. Berhanu, A.L.; Gaurav; Mohiuddin, I.; Malik, A.K.; Aulakh, J.S.; Kumar, V.; Kim, K. A review of the applications of Schiff bases as optical chemical sensors. *TrAC, Trends Anal. Chem.* **2019**, *116*, 74–91. [[CrossRef](#)]
45. Immanuel David, C.; Prabakaran, G.; Nandhakumar, R. Recent approaches of 2HN derived fluorophores on recognition of Al³⁺ ions: A review for future outlook. *Microchem. J.* **2021**, *169*, 106590. [[CrossRef](#)]
46. Zoubi, W.A. Biological Activities of Schiff Bases and Their Complexes: A Review of Recent Works. *Int. J. Org. Chem.* **2013**, *3*, 24. [[CrossRef](#)]
47. Han, X.; Wang, Y.; Huang, Y.; Wang, X.; Choo, J.; Chen, L. Fluorescent probes for biomolecule detection under environmental stress. *J. Hazard. Mater.* **2022**, *431*, 128527. [[CrossRef](#)] [[PubMed](#)]
48. Zhang, Y.; Hao, Y.; Ma, X.; Chen, S.; Xu, M. A dicyanoisophorone-based highly sensitive and selective near-infrared fluorescent probe for sensing thiophenol in water samples and living cells. *Environ. Pollut.* **2020**, *265*, 114958. [[CrossRef](#)] [[PubMed](#)]
49. Lai, X.; Qiu, G.; Ye, Q.; Wang, R.; Liu, J. A reaction-based fluorescent probe for detecting o-phenylenediamine in water and lateritic soil samples. *J. Photochem. Photobiol. A.* **2020**, *386*, 112101. [[CrossRef](#)]
50. Suratsawadee, A.; Wangmo, L.; Ratvijitvech, T.; Siripinyanond, A. A spoilage indicator card based on distance-based color change of paper impregnated with acid-base indicator for freshness monitoring of shrimp. *Microchem. J.* **2022**, *175*, 107110. [[CrossRef](#)]
51. Zhong, K.; Zhou, S.; Yan, X.; Li, X.; Hou, S.; Cheng, L.; Gao, X.; Li, Y.; Tang, L. A simple H₂S fluorescent probe with long wavelength emission: Application in water, wine, living cells and detection of H₂S gas. *Dyes Pigment.* **2020**, *174*, 108049. [[CrossRef](#)]
52. Choudhury, P.; Das, P.K. Progress and trends in self-assembly driven fluorescent organic nanoparticles: A brief overview. *J. Indian Chem. Soc.* **2021**, *98*, 100123. [[CrossRef](#)]
53. Li, J.; Yim, D.; Jang, W.; Yoon, J. Recent progress in the design and applications of fluorescence probes containing crown ethers. *Chem. Soc. Rev.* **2017**, *46*, 2437–2458. [[CrossRef](#)] [[PubMed](#)]
54. Liu, Z.; Zhou, X.; Miao, Y.; Hu, Y.; Kwon, N.; Wu, X.; Yoon, J. A Reversible Fluorescent Probe for Real-Time Quantitative Monitoring of Cellular Glutathione. *Angew. Chem. Int. Edit.* **2017**, *56*, 5812–5816. [[CrossRef](#)] [[PubMed](#)]
55. Niu, L.; Chen, Y.; Zheng, H.; Wu, L.; Tung, C.; Yang, Q. Design strategies of fluorescent probes for selective detection among biothiols. *Chem. Soc. Rev.* **2015**, *44*, 6143–6160. [[CrossRef](#)] [[PubMed](#)]
56. Park, S.; Kwon, N.; Lee, J.; Yoon, J.; Shin, I. Synthetic ratiometric fluorescent probes for detection of ions. *Chem. Soc. Rev.* **2020**, *49*, 143–179. [[CrossRef](#)]
57. Wang, Y.; Zhang, L.; Han, X.; Zhang, L.; Wang, X.; Chen, L. Fluorescent probe for mercury ion imaging analysis: Strategies and applications. *Chem. Eng. J.* **2021**, *406*, 127166. [[CrossRef](#)]
58. Zhang, J.; Wang, N.; Ji, X.; Tao, Y.; Wang, J.; Zhao, W. BODIPY-Based Fluorescent Probes for Biothiols. *Chem.-Eur. J.* **2020**, *26*, 4172–4192. [[CrossRef](#)]
59. Fan, W.; Huang, X.; Shi, X.; Wang, Z.; Lu, Z.; Fan, C.; Bo, Q. A simple fluorescent probe for sensing cysteine over homocysteine and glutathione based on PET. *Spectrochim. Acta A Mol. Biomol. Spectrosc.* **2017**, *173*, 918–923. [[CrossRef](#)]
60. Xu, K.; He, L.; Yang, Y.; Lin, W. A PET-based turn-on fluorescent probe for sensitive detection of thiols and H₂S and its bioimaging application in living cells, tissues and zebrafish. *New J. Chem.* **2019**, *43*, 2865–2869. [[CrossRef](#)]
61. Kumar, P.; Biswas, S.; Koner, A.L. Fast tyrosinase detection in early-stage melanoma with nanomolar sensitivity using a naphthalimide-based fluorescent read-out probe. *New J. Chem.* **2020**, *44*, 10771–10775. [[CrossRef](#)]
62. Zhou, L.; Cui, J.; Yu, Z.; Zou, D.; Zhang, W.; Qian, J. A β-d-galactose-guided fluorescent probe for selectively bioimaging endogenous formaldehyde in living HepG-2 cells. *Sens. Actuators B Chem.* **2021**, *332*, 129494. [[CrossRef](#)]
63. Xiong, K.; Huo, F.; Yin, C.; Yang, Y.; Chao, J.; Zhang, Y.; Xu, M. A off-on green fluorescent chemosensor for cyanide based on a hybrid coumarin-hemicyanine dye and its bioimaging. *Sens. Actuators B Chem.* **2015**, *220*, 822–828. [[CrossRef](#)]

64. Gu, K.; Xu, Y.; Li, H.; Guo, Z.; Zhu, S.; Zhu, S.; Shi, P.; James, T.D.; Tian, H.; Zhu, W. Real-Time Tracking and In Vivo Visualization of β -Galactosidase Activity in Colorectal Tumor with a Ratiometric Near-Infrared Fluorescent Probe. *J. Am. Chem. Soc.* **2016**, *138*, 5334–5340. [[CrossRef](#)] [[PubMed](#)]
65. Liu, F.; Wang, Z.; Wang, W.; Luo, J.; Kong, L. Red-Emitting Fluorescent Probe for Detection of γ -Glutamyltranspeptidase and Its Application of Real-Time Imaging under Oxidative Stress in Cells and in Vivo. *Anal. Chem.* **2018**, *90*, 7467–7473. [[CrossRef](#)]
66. Cho, M.K.; Lim, C.S.; Sarkar, A.R.; Lee, H.W.; Choi, H.J.; Noh, C.; Shin, S.J.; Kim, H.M. A two-photon ratiometric probe for detection of hNQO1 enzyme activity in human colon tissue. *Sens. Actuators Chem.* **2018**, *272*, 203–210. [[CrossRef](#)]
67. Shi, Y.; Huo, F.; Yin, C. Malononitrile as the ‘double-edged sword’ of passivation-activation regulating two ICT to highly sensitive and accurate ratiometric fluorescent detection for hypochlorous acid in biological system. *Sens. Actuators Chem.* **2020**, *325*, 128793. [[CrossRef](#)] [[PubMed](#)]
68. Yu, H.; Fang, Y.; Wang, J.; Zhang, Q.; Chen, S.; Wang, K.; Hu, Z. Enhancing probe’s sensitivity for peroxyxynitrite through alkoxy modification of dicyanovinylchromene. *Anal. Bioanal. Chem.* **2022**, *414*, 6779–6789. [[CrossRef](#)]
69. Wei, L.; Yi, L.; Song, F.; Wei, C.; Wang, B.; Xi, Z. FRET ratiometric probes reveal the chiral-sensitive cysteine-dependent H₂S production and regulation in living cells. *Sci. Rep. UK* **2014**, *4*, 4521. [[CrossRef](#)]
70. Zhang, H.; Liu, R.; Tan, Y.; Xie, W.H.; Lei, H.; Cheung, H.; Sun, H. A FRET-based Ratiometric Fluorescent Probe for Nitroxyl Detection in Living Cells. *ACS Appl. Mater. Inter.* **2015**, *7*, 5438–5443. [[CrossRef](#)]
71. Aron, A.T.; Loehr, M.O.; Bogena, J.; Chang, C.J. An Endoperoxide Reactivity-Based FRET Probe for Ratiometric Fluorescence Imaging of Labile Iron Pools in Living Cells. *J. Am. Chem. Soc.* **2016**, *138*, 14338–14346. [[CrossRef](#)]
72. Jia, X.; Chen, Q.; Yang, Y.; Tang, Y.; Wang, R.; Xu, Y.; Zhu, W.; Qian, X. FRET-Based Mito-Specific Fluorescent Probe for Ratiometric Detection and Imaging of Endogenous Peroxyxynitrite: Dyad of Cy3 and Cy5. *J. Am. Chem. Soc.* **2016**, *138*, 10778–10781. [[CrossRef](#)]
73. Wei, X.; Hu, X.; Zhang, L.; Li, J.; Wang, J.; Wang, P.; Song, Z.; Zhang, J.; Yan, M.; Yu, J. Highly selective and sensitive FRET based ratiometric two-photon fluorescent probe for endogenous β -galactosidase detection in living cells and tissues. *Microchem. J.* **2020**, *157*, 105046. [[CrossRef](#)]
74. Shen, Y.; Zhang, X.; Wu, Y.; Zhang, Y.; Liu, X.; Chen, Y.; Li, H.; Zhong, Y. A lysosome targetable fluorescent probe for palladium species detection base on an ESIPT phthalimide derivative. *Spectrochim. Acta A Mol. Biomol. Spectrosc.* **2018**, *205*, 66–71. [[CrossRef](#)] [[PubMed](#)]
75. Zhou, X.; Liu, Y.; Liu, Q.; Yan, L.; Xue, M.; Yuan, W.; Shi, M.; Feng, W.; Xu, C.; Li, F. Point-of-care Ratiometric Fluorescence Imaging of Tissue for the Diagnosis of Ovarian Cancer. *Theranostics* **2019**, *9*, 4597–4607. [[CrossRef](#)]
76. Ren, H.; Huo, F.; Wu, X.; Liu, X.; Yin, C. An ESIPT-induced NIR fluorescent probe to visualize mitochondrial sulfur dioxide during oxidative stress in vivo. *Chem. Commun.* **2021**, *57*, 655–658. [[CrossRef](#)]
77. Jiang, G.; Zeng, G.; Zhu, W.; Li, Y.; Dong, X.; Zhang, G.; Fan, X.; Wang, J.; Wu, Y.; Tang, B.Z. A selective and light-up fluorescent probe for β -galactosidase activity detection and imaging in living cells based on an AIE tetraphenylethylene derivative. *Chem. Commun.* **2017**, *53*, 4505–4508. [[CrossRef](#)] [[PubMed](#)]
78. Cheng, Y.; Dai, J.; Sun, C.; Liu, R.; Zhai, T.; Lou, X.; Xia, F. An Intracellular H₂O₂-Responsive AIEgen for the Peroxidase-Mediated Selective Imaging and Inhibition of Inflammatory Cells. *Angew. Chem. Int. Ed.* **2018**, *57*, 3123–3127. [[CrossRef](#)]
79. Muthusamy, S.; Yin, S.; Rajalakshmi, K.; Meng, S.; Zhu, D.; Xie, M.; Xie, J.; Lodi, R.S.; Xu, Y. Development of a quinoline-derived turn-on fluorescent probe for real time detection of hydrazine and its applications in environment and bioimaging. *Dyes Pigm.* **2022**, *206*, 110618. [[CrossRef](#)]
80. Gao, M.; Hu, Q.; Feng, G.; Tang, B.Z.; Liu, B. A fluorescent light-up probe with “AIE + ESIPT” characteristics for specific detection of lysosomal esterase. *J. Mater. Chem. B.* **2014**, *2*, 3438–3442. [[CrossRef](#)]
81. Chen, X.; Xu, H.; Ma, S.; Tong, H.; Lou, K.; Wang, W. A simple two-photon turn-on fluorescent probe for the selective detection of cysteine based on a dual PeT/ICT mechanism. *RSC Adv.* **2018**, *8*, 13388–13392. [[CrossRef](#)] [[PubMed](#)]
82. Yang, L.; Su, Y.; Geng, Y.; Zhang, Y.; Ren, X.; He, L.; Song, X. A Triple-Emission Fluorescent Probe for Discriminatory Detection of Cysteine/Homocysteine, Glutathione/Hydrogen Sulfide, and Thiophenol in Living Cells. *ACS Sens.* **2018**, *3*, 1863–1869. [[CrossRef](#)]
83. Zhang, J.; Yang, M.; Mazi, W.; Adhikari, K.; Fang, M.; Xie, F.; Valenzano, L.; Tiwari, A.; Luo, F.; Liu, H. Unusual Fluorescent Responses of Morpholine-Functionalized Fluorescent Probes to pH via Manipulation of BODIPY’s HOMO and LUMO Energy Orbitals for Intracellular pH Detection. *ACS Sens.* **2016**, *1*, 158–165. [[CrossRef](#)] [[PubMed](#)]
84. Callan, J.F.; de Silva, A.P.; Magri, D.C. Luminescent sensors and switches in the early 21st century. *Tetrahedron* **2005**, *61*, 8551–8588. [[CrossRef](#)]
85. Bo, Y.L.; Han, J.A.; Im, J.S.; Morrone, A.; Hwang, E.S. Senescence-associated β -galactosidase is lysosomal β -galactosidase. *Aging Cell* **2006**, *5*, 187–195.
86. Chen, S.; Li, Z.; Li, K.; Yu, X. Small molecular fluorescent probes for the detection of lead, cadmium and mercury ions. *Coordin. Chem. Rev.* **2021**, *429*, 213691. [[CrossRef](#)]
87. Tian, X.; Murfin, L.C.; Wu, L.; Lewis, S.E.; James, T.D. Fluorescent small organic probes for biosensing. *Chem. Sci.* **2021**, *12*, 3406–3426. [[CrossRef](#)] [[PubMed](#)]
88. Yu, F.; Li, P.; Song, P.; Wang, B.; Zhao, J.; Han, K. An ICT-based strategy to a colorimetric and ratiometric fluorescence probe for hydrogen sulfide in living cells. *Chem. Commun.* **2012**, *48*, 2852–2854. [[CrossRef](#)] [[PubMed](#)]

89. Yan, C.; Guo, Z.; Chi, W.; Fu, W.; Abedi, S.A.A.; Liu, X.; Tian, H.; Zhu, W. Fluorescence upconversion enables light-up sensing of N-acetyltransferases and nerve agents. *Nat. Commun.* **2021**, *12*, 3869. [[CrossRef](#)]
90. Wu, L.; Huang, C.; Emery, B.P.; Sedgwick, A.C.; Bull, S.D.; He, X.; Tian, H.; Yoon, J.; Sessler, J.L.; James, T.D. Förster resonance energy transfer (FRET)-based small-molecule sensors and imaging agents. *Chem. Soc. Rev.* **2020**, *49*, 5110–5139. [[CrossRef](#)]
91. Hentze, M.W.; Muckenthaler, M.U.; Andrews, N.C. Balancing acts: Molecular control of mammalian iron metabolism. *Cell* **2004**, *117*, 285–297. [[CrossRef](#)] [[PubMed](#)]
92. He, Y.; Lu, M.; Lu, H.P. Single-molecule photon stamping FRET spectroscopy study of enzymatic conformational dynamics. *Phys. Chem. Chem. Phys.* **2013**, *15*, 770–775. [[CrossRef](#)] [[PubMed](#)]
93. Wallrabe, H.; Periasamy, A. Imaging protein molecules using FRET and FLIM microscopy. *Curr. Opin. Biotech.* **2005**, *16*, 19–27. [[CrossRef](#)] [[PubMed](#)]
94. Coelho, S.; Poland, S.P.; Devauges, V.; Ameer-Beg, S.M. Adaptive optics for a time-resolved Förster resonance energy transfer (FRET) and fluorescence lifetime imaging microscopy (FLIM) in vivo. *Opt. Lett.* **2020**, *45*, 2732–2735. [[CrossRef](#)]
95. Masia, F.; Dewitte, W.; Borri, P.; Langbein, W. uFLIM—Unsupervised analysis of FLIM-FRET microscopy data. *Med. Image Anal.* **2022**, *82*, 102579. [[CrossRef](#)]
96. Weller, A. Über die Fluoreszenz der Salizylsäure und verwandter Verbindungen. *Naturwissenschaften* **1955**, *42*, 175–176. [[CrossRef](#)]
97. Li, J.; Meng, Z. The role of sulfur dioxide as an endogenous gaseous vasoactive factor in synergy with nitric oxide. *Nitric Oxide* **2009**, *20*, 166–174. [[CrossRef](#)]
98. Wang, X.B.; Jin, H.F.; Tang, C.S.; Du, J.B. The biological effect of endogenous sulfur dioxide in the cardiovascular system. *Eur. J. Pharmacol.* **2011**, *670*, 1–6. [[CrossRef](#)]
99. Demchenko, A.P.; Tang, K.; Chou, P. Excited-state proton coupled charge transfer modulated by molecular structure and media polarization. *Chem. Soc. Rev.* **2013**, *42*, 1379–1408. [[CrossRef](#)] [[PubMed](#)]
100. Das, K.; Sappati, S.; Bisht, G.S.; Hazra, P. Proton-Coupled Electron Transfer in the Aqueous Nanochannels of Lyotropic Liquid Crystals: Interplay of H-Bonding and Polarity Effects. *J. Phys. Chem. Lett.* **2021**, *12*, 2651–2659. [[CrossRef](#)]
101. Luo, J.; Xie, Z.; Lam, J.W.Y.; Cheng, L.; Chen, H.; Qiu, C.; Kwok, H.S.; Zhan, X.; Liu, Y.; Zhu, D.; et al. Aggregation-induced emission of 1-methyl-1,2,3,4,5-pentaphenylsilole. *Chem. Commun.* **2001**, *18*, 1740–1741. [[CrossRef](#)]
102. Qiu, Z.; Liu, X.; Lam, J.; Tang, B.Z. The Marriage of Aggregation-Induced Emission with Polymer Science. *Macromol. Rapid Comm.* **2018**, *40*, 1800568. [[CrossRef](#)] [[PubMed](#)]
103. Jiang, X.; Wang, L.; Carroll, S.L.; Chen, J.; Wang, M.C.; Wang, J. Challenges and Opportunities for Small-Molecule Fluorescent Probes in Redox Biology Applications. *Antioxid. Redox Sign.* **2018**, *29*, 518–540. [[CrossRef](#)] [[PubMed](#)]
104. Ball, R.O.; Courtney-Martin, G.; Pencharz, P.B. The In Vivo Sparing of Methionine by Cysteine in Sulfur Amino Acid Requirements in Animal Models and Adult Humans^{1,2}. *J. Nutr.* **2006**, *136*, 1682S–1693S. [[CrossRef](#)]
105. Wang, X.F.; Cynader, M.S. Pyruvate released by astrocytes protects neurons from copper-catalyzed cysteine neurotoxicity. *J. Neurosci.* **2001**, *21*, 3322. [[CrossRef](#)]
106. Ning, Z.; Wu, S.; Liu, G.; Ji, Y.; Jia, L.; Niu, X.; Ma, R.; Zhang, Y.; Xing, G. Water-soluble AIE-Active Fluorescent Organic Nanoparticles: Design, Preparation and Application for Specific Detection of Cysteine over Homocysteine and Glutathione in Living Cells. *Chem.-Asian J.* **2019**, *14*, 2220–2224. [[CrossRef](#)]
107. Yan, L.; Zhang, Y.; Xu, B.; Tian, W. Fluorescent nanoparticles based on AIE fluorogens for bioimaging. *Nanoscale* **2016**, *8*, 2471–2487. [[CrossRef](#)] [[PubMed](#)]
108. Zhang, X.; Zhang, X.; Yang, B.; Zhang, Y.; Liu, M.; Liu, W.; Chen, Y.; Wei, Y. Fabrication of water-dispersible and biocompatible red fluorescent organic nanoparticles via PEGylation of aggregate induced emission enhancement dye and their cell imaging applications. *Colloids Surf. B.* **2014**, *113*, 435–441. [[CrossRef](#)] [[PubMed](#)]
109. Zhang, Y.; Chang, K.; Xu, B.; Chen, J.; Yan, L.; Ma, S.; Wu, C.; Tian, W. Highly efficient near-infrared organic dots based on novel AIE fluorogen for specific cancer cell imaging. *RSC Adv.* **2015**, *5*, 36837–36844. [[CrossRef](#)]
110. Zhao, Q.; Li, K.; Chen, S.; Qin, A.; Ding, D.; Zhang, S.; Liu, Y.; Liu, B.; Sun, J.Z.; Tang, B.Z. Aggregation-induced red-NIR emission organic nanoparticles as effective and photostable fluorescent probes for bioimaging. *J. Mater. Chem.* **2012**, *22*, 15128–15135. [[CrossRef](#)]
111. Li, K.; Qin, W.; Ding, D.; Tomczak, N.; Geng, J.; Liu, R.; Liu, J.; Zhang, X.; Liu, H.; Liu, B. Photostable fluorescent organic dots with aggregation-induced emission (AIE dots) for noninvasive long-term cell tracing. *Sci. Rep. UK.* **2013**, *24*, 635–643. [[CrossRef](#)] [[PubMed](#)]
112. Geng, J.; Zhu, Z.; Qin, W.; Ma, L.; Hu, Y.; Gurzadyan, G.G.; Tang, B.Z.; Liu, B. Near-infrared fluorescence amplified organic nanoparticles with aggregation-induced emission characteristics for in vivo imaging. *Nanoscale* **2014**, *6*, 939–945. [[CrossRef](#)] [[PubMed](#)]
113. Feng, G.; Tay, C.Y.; Chui, Q.X.; Liu, R.; Tomczak, N.; Liu, J.; Tang, B.Z.; Leong, D.T.; Liu, B. Ultrabright organic dots with aggregation-induced emission characteristics for cell tracking. *Biomaterials* **2014**, *35*, 8669–8677. [[CrossRef](#)]
114. Samanta, S.; Gong, W.; Li, W.; Sharma, A.; Shim, I.; Zhang, W.; Das, P.; Pan, W.; Liu, L.; Yang, Z.; et al. Organic fluorescent probes for stochastic optical reconstruction microscopy (STORM): Recent highlights and future possibilities. *Coord. Chem. Rev.* **2019**, *380*, 17–34. [[CrossRef](#)]